STUDY OF CELL MATERIAL INTERACTIONS FOR VASCULAR TISSUE ENGINEERING APPLICATION

A Dissertation

by

XIN QU

Submitted to the Office of Graduate Studies of
Texas A&M University
in partial fulfillment of the requirements for the degree of

DOCTOR OF PHILOSOPHY

May 2011

Major Subject: Chemical Engineering

Study of Cell Material Interactions for Vascular Tissue Engineering Application

STUDY OF CELL MATERIAL INTERACTIONS FOR VASCULAR TISSUE ENGINEERING APPLICATION

A Thesis

by

XIN QU

Submitted to the Office of Graduate Studies of
Texas A&M University
in partial fulfillment of the requirements for the degree of

DOCTOR OF PHILOSOPHY

Approved by:

Chair of Committee,	Mariah Hahn
Committee Members,	Arul Jayaraman
	Victor Ugaz
	Michael McShane
Head of Department,	Michael Pishko

May 2011

Major Subject: Chemical Engineering

ABSTRACT

Study of Cell Material Interactions for

Vascular Tissue Engineering Application. (May 2011)

Xin Qu, B.S., University of Science and Technology of China

Chair of Advisory Committee: Dr. Mariah Hahn

In the US alone, more than 500,000 coronary artery bypass procedures are performed annually. Tissue engineering shows the potential to construct functional grafts to overcome the limited availability of autologous saphenous veins, relatively poor elasticity and low compliance of synthetic materials (mainly Dacron and polytetrafluoroethylene).

In order to meet the low modulus associate with myocyte differentiation, the high suture retention and an ultimate tensile strength (UTS) sufficient to withstand implantation and peak physiological stresses, we designed and characterized a multi-component scaffold comprised of polyurethane electrospun mesh layers bonded together by a fibrin hydrogel matrix. We have demonstrated this composite construct retains the high tensile strength and suture retention strength but displays a “J-shaped” mechanical response similar to that of native coronary artery.

To improve our design, poly(ethylene glycol) diacrylate based hydrogel system was utilized as a blank slate to study the phenotypic regulation by cell material interactions. Fibrinogen, fibronectin, laminin and collagen type IV were incorporated

into the hydrogel to mimic the stimuli from extracellular matrix (ECM) proteins. Surprisingly, no significant effect was detected on induction of smooth muscle cell (SMC) differentiation marker expression, activation of mitogen-activated protein (MAP) kinases pathway, or alteration of surface integrin expression profile. However, fibronectin showed repression of undesired phenotypes in SMC differentiation.

In contrast to ECM proteins, glycosaminoglycans (GAGs) showed more influence on regulating SMC phenotype. By using a scaffold environment intended to be mimetic of early atherosclerosis, the impact of GAG identity on SMC foam cell formation was explored. We focused on chondroitin sulfate C (CSC), dermatan sulfate (DS), and an intermediate molecular weight hyaluronan (HA_{IMW}, ~400 kDa), the levels and/or distribution of which are significantly altered in atherosclerosis. CSC and DS hydrogels were associated with greater SMC phagocytosis of apolipoprotein B than HA_{IMW} gels. However, only SMCs in DS constructs maintained increased expression of adipocyte marker A-FABP relative to HA_{IMW} gels over 35 days of culture.

Combined, our results suggested interesting roles for fibronectin and HA_{IMW} in repression of undesired phenotypes in SMC differentiation, which could give insights into rational design of novel biomaterials for vascular tissue engineering applications.

ACKNOWLEDGEMENTS

I would like to thank my committee chair, Dr. Mariah Hahn, and my committee members, Dr. Jayaraman, Dr. Ugaz, and Dr. McShane, for their guidance and support throughout the course of this research. Thanks also go to my group members, friends, colleagues, and the department faculty and staff, for making my time at Texas A&M University a great experience.

Finally, thanks to my parents for their encouragement and to my wife for her patience and love. I could not have succeeded in this goal without the assistance and support from each of you.

TABLE OF CONTENTS

CHAPTER Page

CHAPTER Page

LIST OF FIGURES

FIGURE Page

LIST OF TABLES

CHAPTER I

INTRODUCTION

Blood vessels form a branched system of arteries and veins to circulate blood from heart to the tissues and organs. Depending on the location and function, blood vessels vary in size, mechanical properties, biochemical content etc. The aorta is the largest artery that transports blood originating from the heart. The smaller muscular arteries are necessary to deliver blood to the tissues and organs, and with the smaller arterioles and the smallest capillaries, blood can be distributed within tissue and organs (1).

In the US alone, the disease of small and medium-sized blood vessels is one of the primary causes of the death (2). Blood vessel replacements are often necessary in the treatment of advanced atherosclerosis, aneurysmal and peripheral vascular disease, etc. For example, in the US alone, more than 500,000 coronary artery bypass procedures are performed annually (3). Although autologous saphenous veins and mammary arteries are the preferred graft materials for these small-caliber vessels (< 6 mm ID), roughly 10 to 20% of patients lack usable tissue (4). Moreover, due to the thrombogenicity, relatively poor elasticity, and low compliance, synthetic materials, such as polyethylene terephthalate (PET) and polytetrafluoroethylene (PTFE) fail as small-caliber vessel replacements, although they show good outcome as peripheral vessel grafts (5). Therefore, an urgent clinical need emerges to find an alternative supply of vessels to

---

This dissertation follows the style of *Tissue Engineering.*

replace diseased arteries. Tissue engineered vascular grafts (TEVGs) represent potential source of alternate prostheses for situations where autologous tissue is unavailable and synthetic prostheses fail (6).

Tissue engineering has already had success in fabricating materials for treatment of chronic wounds and burns, and showed promising results in repair of cartilage defects. But in order to generate appropriate blood vessel replacement by tissue engineering approaches, some substantial challenges need to be faced. First, the construct will have sufficient ultimate tensile strength (UTS) not to burst with changes in blood pressure. Second, the grafts should have elastic wall to withstand cyclic loading, matching compliance with the adjacent host vessel. Third, the grafts should support smooth muscle phenotype and avoid induction of disease phenotypes (1).

1.1 Native Coronary Artery Anatomy

A better understanding of the normal anatomy of the artery, (shown in **Figure 1**), provides the insight for the design of tissue engineered vascular grafts for coronary artery bypass.

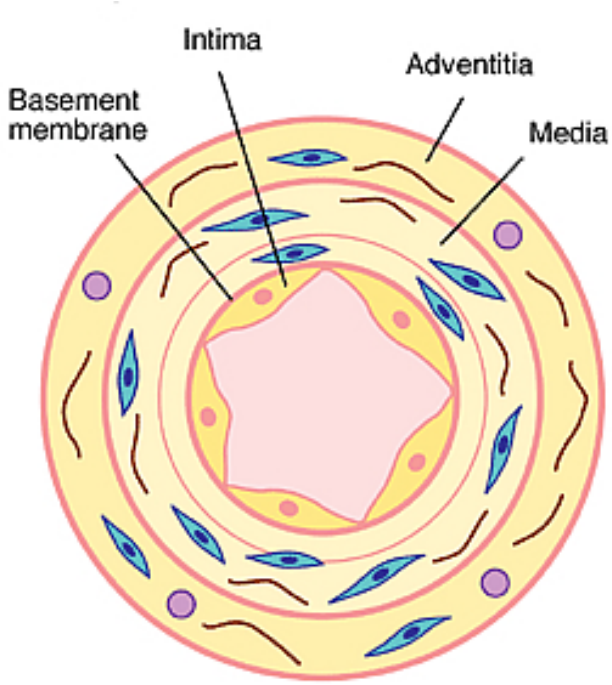

Figure 1. Anatomy of artery wall. (Adapted from Lafleur et al (7))

The artery wall consists of three layers: adventita, media and intima. The outermost adventitia is rich in longitudinal collagen fiber and sometimes fibroblast can be found. The tunica media layer is in the middle of the artery wall and displays mature smooth muscle cells (SMCs) embedded in elastin rich matrix. The media layer is thicker in artery than in the vein and provides elastic response and vasoactivity associated with arterial tissue. The intima is the innermost layer mainly formed by one layer of endothelial cells and performs direct contact with blood.

1.2 Tissue Engineering

Tissue Engineering is an interdisciplinary field that applies the principle of engineering and the life sciences toward the development of biological substitutes that

restore, maintain, or improve tissue function (8). The basic principle of present Tissue Engineering is the combination of appropriate cells with engineered biomaterials under designate conditions that facilitate and lead to tissue formation. In general, three strategies have been used to treat diseased or injured tissues: 1) cellular implantation; 2) tissue implantation; and 3) *in situ* tissue regeneration. For cellular implantation, freshly isolated or cultured cells from the patient or a donor are injected into the defect tissue. Alternatively, some degradable scaffold can be combined with the cells *in vitro* before the implantation too. For the tissue implantation, patient or donor cells can be cultured on a scaffold to create a 3D tissue *in vitro* and then implanted the mature construct to the target tissue. For *in situ* regeneration, the scaffold alone can be injected directly into the defect to promote local tissue repair with the body's own cells (9). In addition to the therapeutic application, tissue engineering can also create model systems *in vitro* for diagnostic applications such as drug metabolism, toxicity.

Biomaterials have been one crucial mainstay of tissue engineering due to the engineering for scaffolds. A tissue engineering scaffold is a material that supports the cells for their growth, proliferation, and differentiation in the absence of native extracellular matrix (ECM). Biomaterial can be fabricated from either natural materials (collagen, alginate) or synthetic polymers (poly ethylene glycol, polylactide). The ideal biomaterial as a scaffold would incorporate specific biochemical cues that could interact with target cells required for repair of damaged tissue. The scaffold could stimulate cell growth after guiding the migration of the target cells into the defect (9).

1.3 Research Plan

My research focuses on study the cell material interactions in smooth muscle differentiation and regulation of smooth muscle phenotype, and applying tissue engineering principles to improve the design of tissue engineering scaffolds for vascular tissue engineering application. The overall approach to this work is outlined below in **Figure 2**.

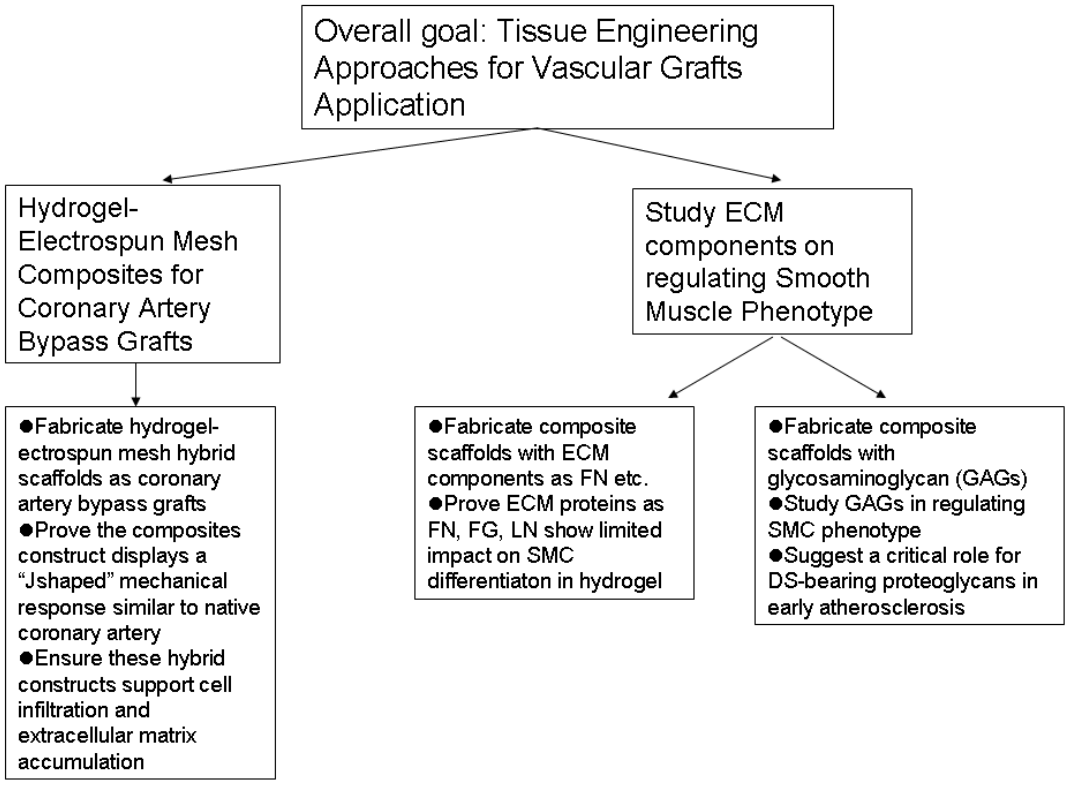

Figure 2. Scope of research.

In order to fabricate the scaffolds suitable for tissue engineered vascular graft, especially coronary artery bypass grafts, the materials should at least meet: 1)

appropriate mechanical response mimicking native vascular tissue; 2) sufficient suture retention strength and an ultimate tensile strength (UTS) to withstand implantation and peak physiological stresses. In the present work, we have demonstrated that a multi-component scaffold comprised of polyurethane electrospun mesh layers (intended to be mimetic of arterial collagen fiber loading) bonded together by a fibrin hydrogel matrix (intended to be mimetic of arterial elastic fiber response) results in a composite construct which retains the high tensile strength and suture retention strength of electrospun mesh but which displays a "J-shaped" mechanical response similar to that of native coronary artery. We also studied the cell-material interactions inside the scaffolds in terms of ECM production and cell infiltration.

In designing tissue engineering vascular grafts, a great challenge is to obtain a well organized and functional media layer which is mainly comprised of mature SMCs. The better understanding of cell-material interactions would be really meaningful to further improve our design of tissue engineered vascular grafts. To study the cell material interactions, we first focused on impact of ECM protein identity on SMC differentiation. Poly (ethylene glycol) diacralyte (PEGDA) gel was used to incorporate ECM proteins, such as fibrinogen, fibronectin, etc, into the scaffold. The differentiation markers and surface integrins as well as cell signaling switches were monitored to assess the cellular behaviors.

Glycosaminoglycans (GAGs) are also critical components in the ECM. It is recognized that GAG retention of lipoproteins is a key event in SMC foam cell formation (10), which is an important phenomena in early atherosclerosis. To explore

the impact of GAG identity on SMC phenotype a scaffold environment was used to be mimetic of early atherosclerosis. Specifically, the effects of chondroitin sulfate C (CSC), dermatan sulfate (DS), and an intermediate molecular weight hyaluronan (HA_{IMW}, ~400 kDa) were examined, as the levels and/or distribution of each of these GAG types are altered in early atherosclerosis.

1.4 Contributions

To the best of our knowledge, the spiral structure of the mesh-hydrogel composites is the first time to be used in tissue engineered grafts, and showed "J-shaped" mechanical response similar to that of native coronary artery in contrast to the conventional bi-layered design that usually displays linear mechanical response. In addition, our study is the first report to utilize three dimensional PEGDA hydrogel system to study impact of ECM components on smooth muscle cell differentiation uncoupling other scaffold properties, such as mesh size, modulus. As discussed below in detail, ECM proteins showed limited impact on smooth muscle differentiation, which was contradicting to several previous studies in two dimensional cell culture system. The discrepancy may suggest the importance of using 3D cell culture system to better probe the natural cell behaviors. Moreover, we have also showed fibronectin and intermediate molecular weight hyaluronan can facilitate the suppression of certain undesired disease phenotypes of smooth muscle cells. These findings could provide important clues to rational design of new biomaterials for vascular tissue engineering applications.

CHAPTER II

HYDROGEL-ELECTROSPUN MESH COMPOSITES FOR CORONARY ARTERY BYPASS GRAFTS*

2.1 Introduction

Each year approximately 500,000 coronary artery bypass procedures are performed in the US alone(3). Although autologous saphenous veins and mammary arteries are the preferred graft materials for these small-caliber vessels (< 6 mm ID), roughly 10 to 20% of patients lack usable tissue(4). Prostheses formed from synthetic materials, such as polyethylene terephthalate (PET) and polytetrafluoroethylene (PTFE), are suitable as peripheral vessel grafts, but fail as small-caliber vessel replacements due to their thrombogenicity, relatively poor elasticity, and low compliance(5). Tissue engineered coronary artery bypass grafts (CABGs) represent a potential source of alternate prostheses for situations where autologous tissue is unavailable and synthetic prostheses fail.

A successful tissue engineered arterial graft must support smooth muscle phenotype while also displaying a suture retention strength and an ultimate tensile strength (UTS) sufficient to withstand implantation and peak physiological stresses. CABGs should also exhibit key features of the "J-shaped," circumferential stress-strain

---

*Reprinted with permission from "Hydrogel-Electrospun Mesh Composites for Coronary Artery Bypass Grafts" by R.E. McMahon, X. Qu, A.C. Jimenez-Vergara, C.A. Bashur, S.A. Guelcher, A.S. Goldstein, M.S. Hahn, 2011. *Tissue Engineering Part C*, 17(4), 451-461, Copyright [2011] by Mary Ann Liebert, Inc. Publishers.

curve characteristic of arteries since the operating stiffness of a vessel modulates its internal stress and mass transport, both of which critically impact vessel health (11). In addition, mechanical mismatch between graft and host tissue at physiological pressures can lead to aneurismal failure (11, 12). In native arteries, this biphasic stress-strain curve arises primarily from the interplay between the collagen and elastic fibers of the arterial medial layer (13), as demonstrated in a classic study by Roach and Burton (13). Specifically, by selectively digesting collagen or elastin from samples of human artery, their individual mechanical roles were elucidated. It was found that the initial "low stiffness" response of the artery wall is dominated by elastic fibers, while the "high stiffness" response observed at increased strains primarily represents the contribution of tensed collagen fibers. The "upturning region" between the "low stiffness" and "high stiffness" segments of the stress-strain curve corresponds to the normal in vivo range of arterial loading and appears to arise from the progressive mechanical recruitment and straightening of collagen fibers with increased arterial distension. This "J-shaped" arterial mechanical response has been difficult to mimic with single component scaffolds (6, 14-16). A multi-component scaffold comprised of interpenetrating layers of a high stiffness and strength material (intended to mimic the contribution of collagen fibers to vessel mechanical response) and a low stiffness material (designed to mimic the mechanical role of elastic fibers) may result in a composite construct that approaches the biphasic, circumferential mechanical response of native vessels while retaining necessary tensile strength and suture retention strength.

In the present work, we investigate the feasibility of this approach through the development and characterization of a composite construct comprised of layers of poly(ester urethane) urea (PEUUR) electrospun mesh bonded together by layers of poly(ethylene glycol) (PEG)-fibrin hydrogel. Electrospun mesh scaffolds were selected for the "high stiffness" component of the composite scaffolds for a number of reasons. First, electrospinning technology is capable of producing nano- and micron-scale fused fiber constructs that display high stiffness and high tensile strength while maintaining open porous networks (17). In addition, the ability to control fiber alignment through modulation of electrospinning conditions can be used to mimic vessel mechanical anisotropy (18). PEUUR elastomers were chosen as the base polymer for the electrospun layers instead of collagen or gelatin due to the greater tunability of PEUUR material properties (19, 20). Specifically, the elastic modulus, strain to failure, UTS, and degradation rate of these elastomers can be broadly tailored through careful control of the chemistry and molecular weight (Mw) of the individual PEUUR segments (20-22). In the current study, the PEUUR polymer formulation and electrospinning conditions were selected based on previous literature (19-24) to yield an oriented mesh scaffold with a directional modulus appropriate to the "high stiffness" region of the coronary artery stress-strain curve.

Similarly, hydrogels were selected for the "low stiffness" component of the hybrid constructs due to the relatively low moduli generally displayed by these materials (25). PEG-fibrin gels in particular were chosen for examination for several reasons. First, the hydrogel component of the proposed composite scaffolds must function to bond

together separate electrospun mesh layers in addition to providing a “low stiffness” response. Fibrin gels have known adhesive properties, and fibrin “glues” have been widely tested for medical applications (26). In addition, fibrin hydrogels have been previously shown to hold promise as tissue engineered vascular graft scaffolds (27-30)and are believed to support the elastogenesis important to the maintenance of long-term graft mechanical properties (29). In the present work, the fibrin hydrogel composition was selected based on previous literature (27-30) to display a low-strain elastic modulus appropriate to the initial toe region of the coronary artery stress-strain curve. PEG chains were grafted onto the fibrin gel network to modulate its degradation rate (31, 32). We demonstrate that the composite scaffolds prepared by bonding together layers of the selected PEUUR mesh with the PEG-fibrin hydrogel matrix exhibited a “J-shaped” stress-strain response similar to that of native human coronary artery. Moreover, we show that these hybrid constructs display suture retention strengths and UTS appropriate for implantation at the time of preparation while supporting longer-term cell infiltration and extracellular matrix accumulation.

2.2 Materials and Methods

2.2.1 Poly(ethylene glycol) Diacrylate Synthesis

Diacrylate-derivatized PEG (PEGDA) was prepared as previously described by combining 0.1 mmol/mL dry PEG (3.4 kDa; Sigma), 0.4 mmol/mL acryloyl chloride (Sigma), and 0.2 mmol/mL triethylamine (Sigma) in anhydrous dichloromethane (DCM; Fisher Scientific) and stirring at 4 °C under argon overnight (33). The resulting solution

was washed with 2 M K_2CO_3 and separated into aqueous and DCM phases to remove HCl. The DCM phase was subsequently dried with anhydrous $MgSO_4$, and PEGDA was precipitated in diethyl ether (Fisher Scientific), filtered, and dried under vacuum.

2.2.2 Electrospun Mesh Fabrication

PEUUR Synthesis. A linear segmented degradable PEUUR elastomer, consisting of an alternating poly(ε-caprolactone) (PCL) soft segment and a urethane- and urea-containing hard segment, was synthesized using a standard two-step technique in a three-neck, round-bottom flask equipped with argon inlet and outlet, condenser, and stirrer (34). First, the flask was charged with anhydrous dimethyl sulfoxide (DMSO; Acros Organics) and 1,6-diisocyanatohexane (HDI; Sigma-Aldrich), immersed in a 75 ^{o}C oil bath and purged with argon. Next, PCL diol (average Mw 2000 Da, PCL2000; Sigma) that had been dried for 24 h at 80 °C under vacuum and dissolved in DMSO was charged into the reactor. The prepolymer content in the reactor was controlled at 14 wt%, and the relative masses of HDI and PCL2000 were selected to achieve a prepolymer NCO:OH equivalent ratio of 2.0:1.0. Dibutyltin dilaurate (Sigma) was added to the flask at 1000 ppm, and the reaction was allowed to proceed for 3 h to produce an HDI.PCL2000.HDI prepolymer. In the second step, a solution of 1,3-propanediol bis(4-aminobenzoate) (Sigma) in DMSO was prepared at 50 °C and added to the reaction vessel. The NCO:OH equivalent ratio of the polyurethane was controlled at 1.03:1.0, and the polymer concentration was 12 wt%. Dibutyltin dilaurate was added to a concentration of 1000 ppm. The reaction was allowed to proceed at 80 ^{o}C for 20 h. The

final polymer, PEUUR2000, was then precipitated in diethyl ether (Sigma) and dried for 24 h at 8 °C under vacuum.

Electrospinning Procedure. The PEUUR2000 was electrospun to form fused-fiber meshes with controlled fiber diameter and fiber alignment as described previously (34). Briefly, electrospinning was performed with a 10 wt% PEUUR2000 solution in 50:50 isopropanol:1,1,1,3,3,3-hexaflouro-2-propanol (HFIP; Sigma) using a 22-gauge Teflon tipped needle, a 15 kV potential, a throw distance of 15 cm, and a syringe flow rate of 3 mL/h. A 6-cm-diameter drum rotating at a linear velocity of 7.9 m/s served as the collector, and spinning time was selected to yield mesh sheets of ~80 μm thickness. Meshes were removed from the drum and soaked in ethanol for 7 days followed by soaking in deionized water for 2 days to remove residual HFIP. The meshes were then dried followed by sterilization using a Co-60 γ-irradiator (Model 484R, JL Shepherd and Associates).

2.2.3 Electrospun Mesh Characterization

Fiber Diameter and Alignment. The mean diameter and angular deviation of fibers within the electrospun mesh sheets were determined by quantitative analysis of scanning electron microscopy (SEM) images. Briefly, electrospun meshes were mounted onto studs and sputter-coated with Pd. Images were acquired using a LEO 1550 Field Emission SEM (Carl Zeiss SMT) operating at 5 kV. Resultant images were imported into ImagePro Plus software (ICube), and fiber diameter and angle of orientation were determined per Bashur et al (34).

Mechanical Testing of Electrospun Mesh Rings. To permit direct comparison of mesh mechanical properties with those of the tubular hydrogel-mesh composites, rectangular 1.5 cm x 3.5 cm mesh strips were cut with the short edge parallel to the direction of fiber alignment. These stripes were subsequently wrapped around a 4 mm glass rod so as to give circumferentially-oriented fibers. The seam of the wrapped mesh was temporarily secured with knotted Dacron thread, and 0.3 μL of 50:50 isopropanol:HFIP was pipetted at ~ 3 mm intervals along the mesh seam. The solvent locally dissolved the mesh fibers but not the Dacron string. The dissolved mesh fibers reset as the solvent evaporated to form a cohesive tubular mesh.

Five ring segments 3-5 mm in width were cut from the resultant mesh, after which the segments were wetted in PBS. Circumferential mechanical tests were performed using a modification of the ring testing technique validated in Johnson et al (35). In brief, each segment was mounted onto an Instron 3342 using custom brackets (36). The ring segments were exposed to uniaxial strain at a rate of 6 mm/min until failure. Applied stress was calculated from the measured force by approximating the area of force application as two rectangles, each with sides equal to the width and wall thickness of the ring. The gauge length was taken as the mid-wall construct diameter, Dv, which was defined as inner diameter of the unstretched ring plus the wall thickness, hv. The UTS was defined as the maximum stress applied prior to failure. The tangential modulus of each ring mesh sample was defined as the slope of the resulting stress–strain curve at a reference stress of 330 kPa. This reference stress was selected to represent the

circumferential stress, $\sigma\theta$, that would be experienced by vessels of similar dimensions at physiological pressures ($\sigma\theta \sim 0.5PavgDv/hv$, Pavg ~ 100 mmHg) (35).

2.2.4 PEG-Fibrin Hydrogel Fabrication and Characterization

Based on the modulus of the "low stiffness" region of the coronary artery stress-strain curve (12) and based on previous fibrin hydrogel literature (27-30), a 3 wt% fibrin gel was selected for examination. To fabricate these hydrogels, sterile-filtered thrombin (Sigma) was added to sterile-filtered, human fibrinogen (MP Biomedicals) in PBS to achieve a 3 wt% fibrinogen solution containing 5 U/mL thrombin. The resulting solution was rapidly pipetted into separate wells of a 12 well plate. Following 30 min incubation at room temperature, the gels were immersed in PBS containing 1.3 U/mL thrombin, 0.5 wt% 3.4 kDa PEGDA, and 0.26% photoinitiator (Irgacure 2959; Ciba). After 1 h at 37 °C, the hydrogels were removed from the thrombin-PEGDA solution and exposed to longwave UV light (~10 mW/cm2; UVP) for 5 min. The extended thrombin exposure was intended to increase fibrin crosslinking and therefore to increase the mechanical strength of the network. In addition, since PEG-grafting to protein networks has been demonstrated to reduce the rate of protein degradation (31), PEGDA and photoinitiator were incorporated into the immersion solution to enable PEG conjugation to the fibrin gel. To ensure PEG-grafting to the fibrin network rather than the formation of interpenetrating fibrin and PEGDA hydrogel networks, the concentration of PEGDA in the immersion solution was maintained below the level required to support hydrogel formation. The ability of acrylate-terminated PEG to conjugate to the fibrin network was confirmed using a fluorescently-labeled monoacrylate-derivatized PEG (data not shown).

To mechanically test the PEG-fibrin gels, 6 mm punches were cored from the central region of each 22 mm hydrogel disc and mounted onto an Instron 3342. Following application of a 0.05 N preload, each hydrogel was subjected to unconfined compression at a strain rate of 1 mm/min from 0 to 25% strain.

2.2.5 Cell Culture

Mouse smooth muscle progenitor cells (10T½, American Type Culture Collection) at passage 2 were thawed and expanded at 37 °C and 5% CO2. During expansion, cells were cultured in Dulbecco's Modified Eagle's Medium (DMEM; Mediatech) containing 10% heat-inactivated fetal bovine serum (FBS; Hyclone). Cells were harvested for seeding and/or encapsulation between passages 10 and 12.

2.2.6 Hybrid Hydrogel-Mesh Construct Fabrication

To fabricate tubular hybrid constructs, molds were employed that consisted of a Teflon base, an outer hollow cylinder of Teflon (~5.5 mm ID, 0.30 mm wall thickness; Small Parts, Inc.), and an inner, thin-walled latex tube (~3.25 mm OD, 0.38 mm wall thickness; Kent Elastomers) supported by a 2 mm glass rod. All mold components were sterilized by autoclaving. Each construct was fabricated in a three-step process shown schematically in (**Figure 3A**). In brief, rectangular segments (2 cm × 3.5 cm) were cut from the electrospun mesh sheets such that the short edge of the rectangle was parallel to the average direction of fiber orientation. Next, each mesh segment was exposed to media containing 40% serum overnight at room temperature to improve cell adhesion. The coated mesh segments were then rinsed with PBS, and cells were seeded on the

upper mesh surface at 10^4 cells/cm^2. Following two days of culture, the cell-laden meshes were rolled around the latex mandrels (**Figure 3A**), resulting in ~2 concentric mesh layers and a mean circumferential orientation of the mesh fibers. During the rolling process, the cell layer faced outward and mesh segments were handled only at the edges to limit mechanical removal of seeded cells. Sterile-filtered thrombin and harvested 10T½ cells were added to sterile-filtered human fibrinogen in PBS to achieve a final solution containing 3 wt% fibrinogen, 5 U/mL thrombin, and $5x10^6$ 10T½ cells/mL. Immediately following the addition of thrombin, the fibrinogen-cell suspension was rapidly pipetted around the inner, mesh-wrapped mandrel. The thrombin content of this fibrinogen solution had previously been tuned to provide the relatively slow polymerization rate needed to allow fibrinogen to impregnate the mesh layers prior to polymerization while simultaneously resulting in a hydrogel of sufficient mechanical strength to permit removal of an intact hydrogel-mesh composite from the mold. Following 30 min incubation at room temperature, the constructs were removed from the molds and immersed in PBS containing 1.3 U/mL thrombin, 0.5 wt% 3.4 kDa PEGDA, and 0.26% Irgacure 2959. After 1 h at 37 °C, the constructs were removed from the thrombin-PEGDA solution, and exposed to longwave UV light (~10 mW/cm2, UVP) for 5 min. The resulting constructs (~3.5 cm length, ~5.5 mm OD, ~1 mm thickness) were then immersed in media containing 10% FBS and 1% PSA (10 U/L penicillin, 10 g/L streptomycin, and 25 mg/L amphotericin; Mediatech). In addition, 1 ng/mL transforming growth factor β1 (TGF-β1; Sigma) was added to the culture media to promote 10T½ differentiation into smooth muscle-like cells (37, 38).

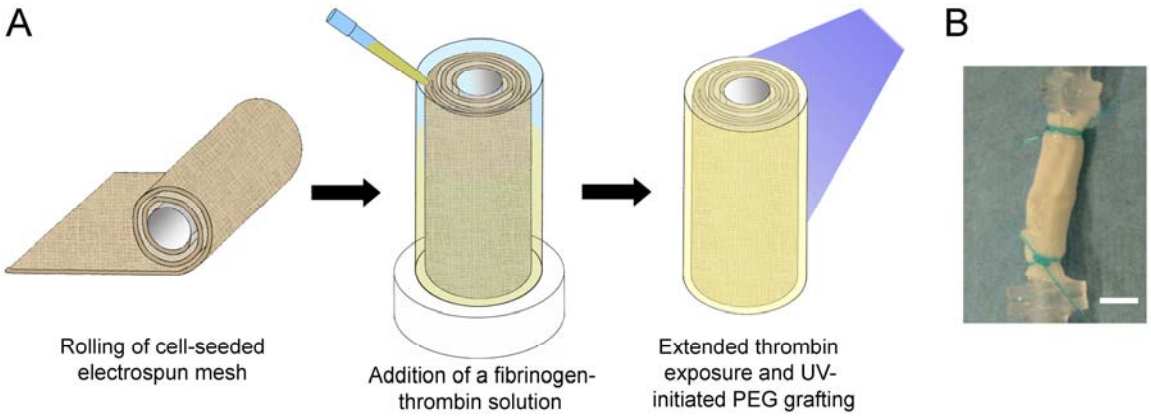

Figure 3. Hybrid hydrogel-mesh construct fabrication. (A) A schematic demonstrating construct fabrication procedure. Briefly, a cell-seeded electrospun mesh is wrapped around a hollow latex mandrel, followed by mold assembly and the addition of a fibrinogen-thrombin hydrogel precursor solution which impregnates the mesh layers as the fibrinogen polymerizes. The resulting fibrin mesh construct is then removed from the mold, after which thrombin exposure is repeated and PEGDA is grafted to the fibrin network. (B) An image of a PEG-fibrin mesh composite construct mounted onto the ports of a pulsatile bioreactor construct chamber and secured with Dacron thread. Scale bar = 5 mm.

2.2.7 Time-Zero Construct Analyses

Following 24 h of additional culture, 3-5 mm ring segments were harvested from the hybrid gel-mesh constructs for tangential modulus, UTS, and suture retention strength measurements. In addition, separate segments were collected for cell viability assessment and SEM imaging. The inner latex tubing was gently removed prior to performance of these tests.

Mechanical Property Assessment. Circumferential mechanical tests were conducted on ~3 mm hybrid scaffold ring segments (n = 4). These tests were performed per the methodology described for the tubular mesh ring segments, except that the

tangential modulus of each sample was defined as the slope of the stress–strain curve at a reference stress of 30 kPa rather than 330 kPa. As previously discussed, the reference stress was selected to represent the circumferential stress that would be experienced by vessels of similar dimensions at Pavg ~ 100 mmHg ($\sigma\theta \sim 0.5PavgDv/hv$) (35). Thus, this shift in reference stress reflects the shift in construct dimensions between the mesh-only scaffolds and the hybrid gel-mesh constructs.

For assessment of suture retention strength, ~5 mm hybrid construct ring segments were glued along their cylindrical base to rectangular pieces of wood using cyanoacrylate-based glue. Each wood piece was subsequently clamped to the lower grip of an Instron 3342. A loop of 5–0 PDSTM suture (Ethicon) was created ~2 mm from the upper edge of each sample and secured to the upper clamp of the testing device. The force required to pull-out the suture was monitored at a constant cross-head speed of 150 mm/min. Suture retention strength was considered to be the maximum force recorded prior to suture pull-through and was examined for n = 4 specimens.

Cell Viability Analysis. To confirm the cytocompatibility of the extended thrombin-PEGDA exposure associated with hybrid gel-mesh construct fabrication, LIVE-DEAD staining (Invitrogen) was performed per standard protocols for n = 3 specimens.

SEM Analysis. To examine the interpenetration of the fibrin gel and electrospun mesh components of the composite constructs, ring segments were fixed in 10% acrolein (Sigma) and dehydrated with a graded ethanol series (5-100%) with intermittent vacuum in a PELCO Biowave® microwave system (Ted Pella, Inc.) at 200 W and 10 °C. One

min microwave cycles were used for dehydration until 50% ethanol, after which 6 min cycles were used to complete the dehydration process. Final dehydration consisted of three changes of 100% ethanol with intermittent vacuum and 6 min microwave cycles. Ethanol was then replaced with three changes of hexamethyldisilizane (Electron Microscopy Sciences) followed by the intermittent vacuum and microwave cycles. The resulting ring segments were mounted along their base onto stubs, after which they were exposed to ruthenium tetroxide vapor (Sigma), sputtercoated with Au:Pd (60:40), and imaged in a JEOL 6400 SEM equipped with a tungsten filament at an accelerating voltage of 10 kV.

2.2.8 Exposure of Hydrogel-Mesh Constructs to Physiological Pulsation

Remaining hybrid hydrogel-mesh constructs were cultured statically for 2 days following initial fabrication, after which each construct was cut in half using sterile surgical scissors (resulting in a series of constructs ~1.5 cm in length). One half of each construct was randomly assigned for dynamic culture, while the remaining portion was allocated for static culture. Dynamic constructs were mounted in the construct chamber of a modified version of the pulsatile flow bioreactor previously described in Bulick et al (36). The low-stiffness, thin-walled latex tubing employed as the inner mandrel during composite construct fabrication ensured the formation of a tight seal between the graft lumen and the construct chamber ports per Syedain et al (39). The end-segments of the mounted constructs were then further secured with sterile Dacron thread (**Figure 3B**), and fluid flow through the constructs was increased until luminal pressures of ~85 mmHg were achieved. Pulsation (ΔP ~ 20 mmHg at 60 beats per min) was initiated

using a CellMax pump (Spectrum Labs). The pressure waveforms experienced by the constructs were monitored using pressure transducers (Merit Medical) placed immediately upstream and downstream of each construct. Each pressure transducer was equipped with a valve, which was used to match resistances in the construct lines.

During the period of mechanical conditioning, both static and dynamic constructs were cultured in DMEM, 10% FBS, 1% PSA, 1 ng/mL TGF-β1, with 2 mg/mL ε-aminocaproic acid to slow fibrin degradation, and 50 μg/ml ascorbic acid to increase collagen production. Media was changed for all constructs every two days for 12 days. To estimate the circumferential strain experienced by the constructs during mechanical conditioning, the measured tangential moduli (E) and vessel dimensions were input into the Bernoulli equation $\Delta\varepsilon \sim \frac{0.5(\Delta P)D_v}{h_v E}$, with D_v and h_v as previously defined (40). Although the Bernoulli equation does not account for the structural inhomogeneity of the fibrin-mesh constructs, it served as an initial estimate of the strains experienced within the construct due to the applied cyclic loads.

2.2.9 Endpoint Construct Analyses

Following 16 days of total culture (16 days = 2 days of culture prior to mesh rolling + 2 days post-rolling but prior to static versus dynamic allocation + 12 days post-onset of mechanical conditioning), each PEG-fibrin-mesh construct was cut into 5 ring segments, each ~3 mm in length. The two end-segments were discarded, and the inner latex tubing was gently removed from the remaining segments. One segment per construct was allocated for mechanical testing. The remaining sections were allocated

for histological or biochemical assays. Endpoint scaffold tangential modulus and UTS assessments were performed as for the 24 h constructs. Details of the biochemical and histological analyses are given in the following sections.

Biochemical Analyses. Samples for biochemical analyses were transferred to 2 mL screw-cap microfuge tubes containing 1 mL of 3.2 mm stainless steel beads (Biospec) and 1.5 mL of lysis buffer (PBS containing 1% Triton X-100 (Fisher), 0.5% sodium dodecyl sulfate (Sigma), and 100 μg/mL phenylmethanesulfonylfluoride (Sigma)). Each sample segment was homogenized at 4800 rpm in a Bead-Beater homogenizer (Biospec) in 10 sec cycles with 1 min intermediate cooling on ice. The homogenate was then clarified by centrifugation, and aliquots of the supernatant were stored at -80 °C. At the time of analysis, thawed aliquots were evaluated via competitive ELISA for arterial ECM proteins collagen I (COL1A1; clone D-13), collagen III (COL3A1; clone S-17), and elastin (clone BA-4). In addition, the housekeeping protein GAPDH (clone V-18) and smooth muscle cell (SMC) markers calponin h1 (clone N-15) and SM22α (clone P-15) were examined.

Competitive ELISAs were conducted per standard procedures. In brief, blocking peptides for each antibody, except for the elastin antibody, were obtained from Santa Cruz Biotechnology (SCBT). For the elastin antibody, bovine α-elastin (Sigma) was used as a source of blocking peptides. EIA plates (Costar) were coated with the appropriate peptide at either 500 ng/well (collagen III peptide) or 2000 ng/well (collagen I, calponin h1, SM22α, α-elastin, GAPDH peptides). Coated wells were then blocked with bovine serum albumin (BSA) and rinsed with PBS. Aliquots of each sample were

incubated with primary antibody (SCBT) for 1 h, after which the sample-antibody mixtures were applied to coated wells for 1 h. Standard curves were similarly prepared by incubating primary antibody with varying levels of blocking peptide for 1 h, followed by solution application to coated wells. For both samples and standards, primary antibody which had bound to the coated well surface was detected using an appropriate HRP-conjugated secondary antibody (Jackson Immunoresearch), followed by application of 2,2'-azino-bis(3-ethylbenzthiazoline-6-sulphonic acid) (Sigma) and monitoring of absorbance at 410 nm. Each target protein was as analyzed in duplicate for each sample (n = 8 samples per treatment group).

Histological Analyses. Histological segments were formalin-fixed, embedded in OCT media, and cut into 10 μm transverse sections which were mounted onto charged glass slides. Standard immunostaining protocols were employed. In brief, rehydrated sections were blocked by 30 min exposure to Terminator (Biocare Medical). Primary antibodies for collagen I (Rockland Immunochemicals), collagen III (Rockland Immunochemicals), and SM22α (clone P-15; SCBT) were diluted in PBS containing 3 % BSA and 0.5 % Tween 20 and applied overnight at 4 °C. Bound primary antibody was detected using an appropriate HRP-conjugated secondary antibody (Jackson Immunoresearch) followed by application of the chromogen 3,3’-diaminobenzidine (Biocare Medical). Stained sections were then dehydrated with graded alcohol, transferred to xylene, and coverslipped using either Polymount (Polysciences) or Curemount (Instrumedics). Stained sections were imaged using an Axiovert microscope (Zeiss). Cryosections of static and dynamic samples exposed to species-specific IgG

control serum in place of primary antibody served as negative controls for each immunostaining procedure.

2.2.10 Statistical Analyses

Data are reported as mean ± standard error of the mean. Comparison of sample means was performed by one-way ANOVA using SPSS software, $p < 0.05$.

2.3 Results

2.3.1 Electrospun Mesh and PEG-Fibrin Hydrogel Characterization

PEUUR mesh sheets were prepared using spinning conditions intended to yield 1-2 μm fiber diameters, relatively high fiber alignment, and ~80 μm thick sheets. SEM imaging of the resulting mesh layers revealed a mean fiber diameter of 1.07 ± 0.35 μm, a fiber angular deviation of ~21° (indicative of highly aligned fibers), and a mesh thickness range of ~60-100 μm (**Figure 4A**). To permit direct comparison of mesh mechanical properties with those of the tubular hydrogel-mesh composites, tubular mesh scaffolds with mean circumferential fiber orientation were prepared. Ring segments from the tubular mesh constructs were mechanically tested and displayed an average UTS of 0.70 ± 0.24 MPa and an average tangential modulus of 0.92 ± 0.24 MPa. **Figure 5A** compares the circumferential stress-strain behavior of the tubular PEUUR electrospun mesh with that of a representative human coronary artery. **Figure 5B** illustrates the contribution of elastin and collagen to the arterial loading response, as determined by Roach and Burton (13). Examination of **Figures 5A** and **5B** indicates that the circumferential mechanical response of the tubular mesh scaffolds agreed well with the

"high stiffness" segment of the coronary artery stress-stain curve and with the contribution of collagen to the arterial mechanical response. Similarly, mechanical testing of the selected PEG-fibrin hydrogel formulation revealed a stress-strain curve that closely mimicked the contribution of elastin to the "low stiffness" region of the arterial stress-strain curve (**Figures 5A-B**).

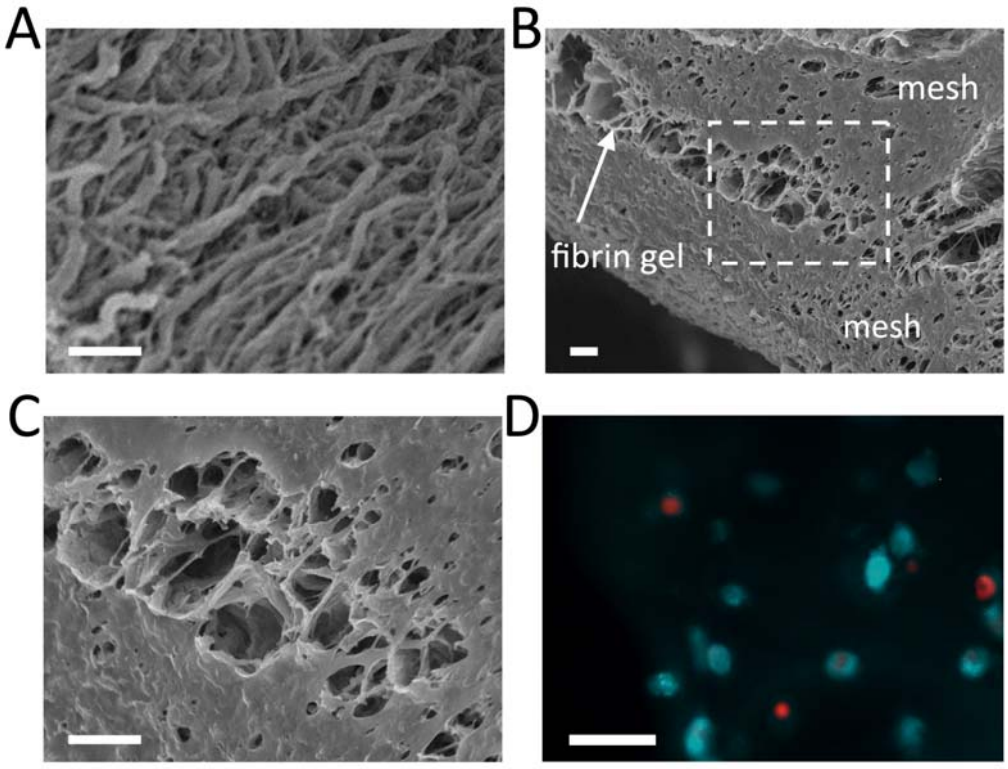

Figure 4. Construct structural integrity and cell viability. (A) An SEM image of a single electrospun mesh layer illustrating fiber thickness and orientation. (B) An SEM image of a transverse cross-section through a hydrogel-electrospun mesh construct indicating effective bonding and interpenetration between the hydrogel and mesh layers. In preparation for SEM imaging, the inter-layer bond withstood dehydration (which differentially impacts hydrogel and mesh components) as well as multiple microwave cycles. (C) A higher magnification image of the boxed region of the hydrogel-mesh construct shown in (B). (D) A representative fluorescence image of LIVE (green)-DEAD (red) stained cells within the fibrin gel portion of the hybrid constructs at 24 h post-fabrication. As shown in (D), cells encapsulated within the fibrin hydrogel had not yet fully spread following 24 h of culture. The scale bars in (A)-(C) represent 10 μm and the scale bar in (D) represents 40 μm.

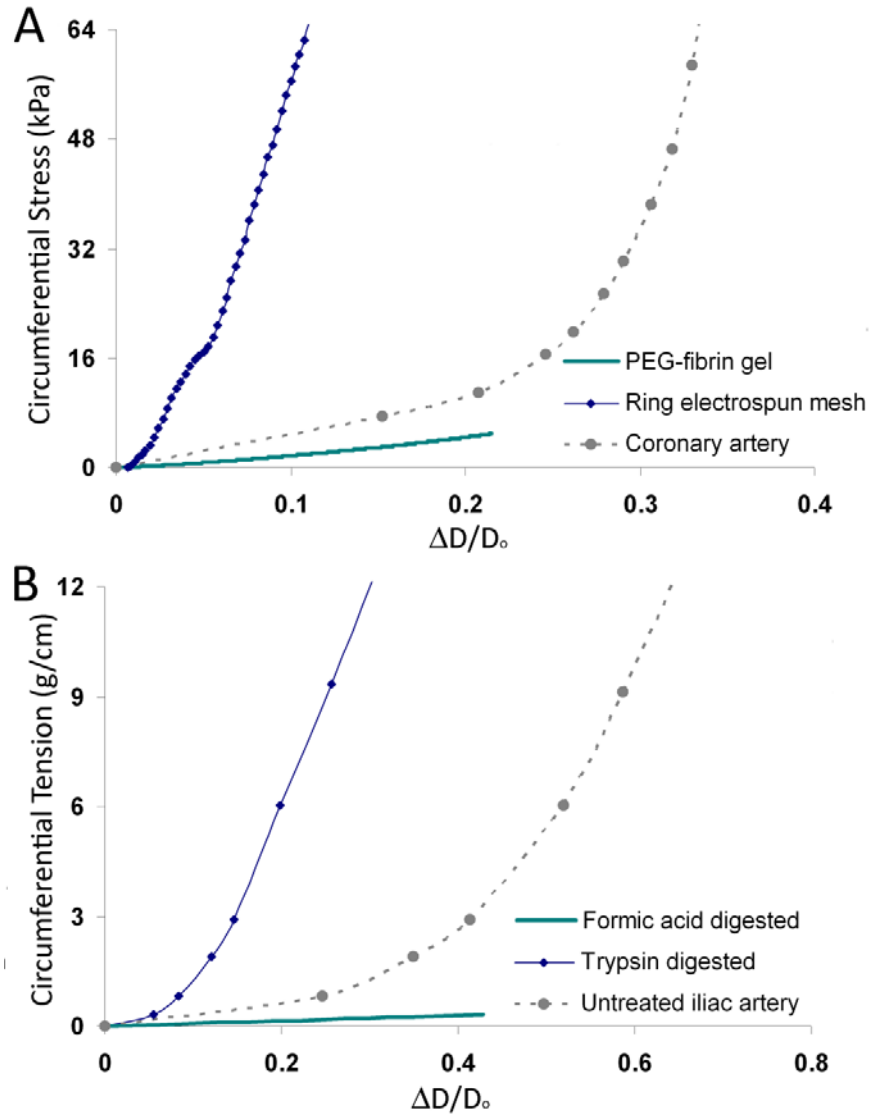

Figure 5. Arterial, PEG-fibrin, and PEUUR electrospun mesh mechanical responses. (A) A representative circumferential stress-strain response for human coronary artery, adapted from van Andel et al (12). In the present study, the PEUUR formulation and electrospinning conditions were selected to result in a mesh which would mimic the contribution of collagen fibers to the "high stiffness" region of the coronary artery stress-strain curve, as shown in (B). The PEG-fibrin hydrogel formulation was similarly selected to mimic the contribution of elastic fibers to the "low stiffness" region of the stress-strain curve, as illustrated in (B). (B) The circumferential tension-strain response of a human iliac artery and the respective contributions of elastin and collagen, adapted from Roach and Burton (13). The trypsin digested specimen represents the influence of the loss of elastin on arterial dynamics. Alternatively, the formic acid digested sample represents the impact of the removal of collagen fibers.

2.3.2 PEG-Fibrin-Mesh Construct Fabrication and Assessment of Cell Viability

Given the correspondence in mechanical responses described above, composite grafts were prepared using the selected PEURR electrospun mesh and PEG-fibrin formulation. In addition to providing the "low stiffness" response of the composite scaffold, the PEG-fibrin hydrogel was intended to act as an adhesive agent, effectively bonding successive mesh layers together. To serve as an effective bonding agent, the fibrin hydrogel should penetrate into the electrospun mesh layers. SEM imaging was therefore conducted to assess the microstructure of the PEG-fibrin mesh composites. The resulting images indicate that the chosen construct fabrication conditions supported the hydrogel-mesh interpenetration required for construct integrity and for the effective transfer of load between scaffold components (**Figures 4B-C**). To confirm the cytocompatibility of the extended exposure to thrombin, PEGDA, and photoinitiator associated with construct generation, the LIVE-DEAD assay was performed on scaffold segments (**Figure 4D**). These studies indicated a 24 h post-fabrication cell viability of 75 ± 2%, a level consistent with that observed following cell encapsulation within PEGDA gels (41).

2.3.3 Assessment of PEG-Fibrin-Mesh Construct Mechanical Properties

To assess the potential of composite grafts to be implanted at the time of fabrication, the suture retention strength of the PEG-fibrin-mesh constructs was determined. These measures indicated an average suture retention strength of 1.16 ± 0.08 N. In addition, the mechanical response of hybrid gel-mesh scaffolds to circumferential loading was characterized both at 24 h post-fabrication and following 16 days of total

culture. As illustrated in **Figure 6**, the composite constructs displayed a "J-shaped" stress-strain curve, with the region of "upturning" occurring at similar strains as for native human coronary artery (**Figure 6** versus **Figure 5A**). In addition, the stress-strain behavior of the PEG-fibrin hydrogel and the electrospun mesh components correlated well with the "low stiffness" and "high stiffness" regions, respectively, of the composite construct stress-strain curve. Since mechanical mismatch between vascular grafts and native tissue over the range of normal physiological loading can result in aneurysmal failure, the average tangential modulus of the hybrid scaffolds was evaluated at a circumferential stress corresponding to normal physiological pressures (**Figure 6**). The average tangential modulus of the hydrogel-mesh constructs 24 h post-fabrication was 0.48 ± 0.03 MPa, approximately 50% lower than the corresponding tangential modulus of the tubular mesh-only scaffolds. Similarly, the endpoint tangential moduli of the static and dynamic hybrid constructs were 0.57 ± 0.13 MPa and 0.57 ± 0.15 MPa, respectively, values statistically indistinguishable from that of the 24 h composite grafts. For the purpose of comparison, the tangential modulus represented by the human coronary artery stress-strain curve in **Figure 5A** was calculated to be ~0.34 MPa.

In terms of tensile strength, the 24 h hydrogel-mesh constructs displayed an average UTS of 0.32 ± 0.06 MPa. This UTS value was approximately 50% of that of the tubular mesh scaffolds and likely reflects the fact that composite construct failure arises from breakdown of the mesh-hydrogel bonding rather than from internal mesh failure. The average endpoint UTS of the statically-cultured composite scaffolds was similar to that of the 24 h hybrid grafts at 0.28 ± 0.08 MPa. In contrast, the average UTS of

mechanically-conditioned scaffolds was 0.10 ± 0.06 MPa, or roughly 33% of the 24 h construct UTS ($p = 0.048$).

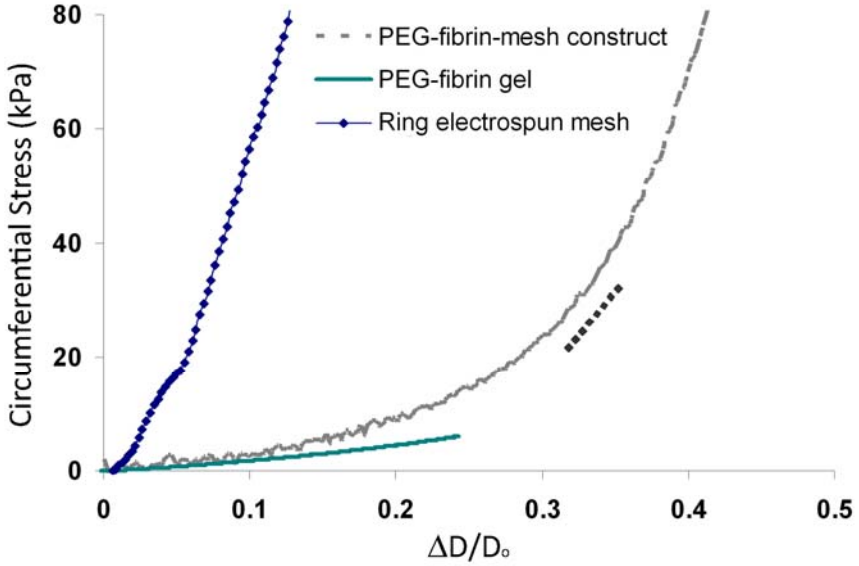

Figure 6. A representative circumferential stress-strain response of a hydrogel-electrospun mesh scaffold relative to the mechanical responses of the individual construct components. The slope of the dashed line represents the tangential modulus of the composite constructs at physiological pressures.

2.3.4 ECM and Cell Phenotype Analyses

In order to examine cell phenotype and ECM production within the PEG-fibrin-mesh composites, competitive ELISA assays and immunohistology were performed. Although immunohistology indicated a similar staining intensity for SMC marker SM22α on a per cell basis in both static and dynamic constructs, marked differences in the distribution of stained cells were observed between these construct types (**Figure 7**). Since TGF-β1 treatment has been previously shown to induce > 90% of exposed 10T½ cells to express early- and mid-term SMC markers (38), the distribution of SM22α-stained cells within the mesh layers could be taken as an indicator of the extent of cell

migration into the composite construct mesh. At the time of hybrid scaffold fabrication, cells were primarily localized at the mesh surface (**Figure 7A**), consistent with the initial mesh seeding conditions. Following 16 days of total culture, cell migration into the mesh layers of the static hybrid constructs tended to be limited to the first ~15 μm of the seeded surface of each mesh layer (**Figure 7B**). In contrast, the average dynamic scaffold exhibited cell migration into the first ~35 μm of the seeded surface of each mesh layer at 16 days of culture (**Figure 7C**).

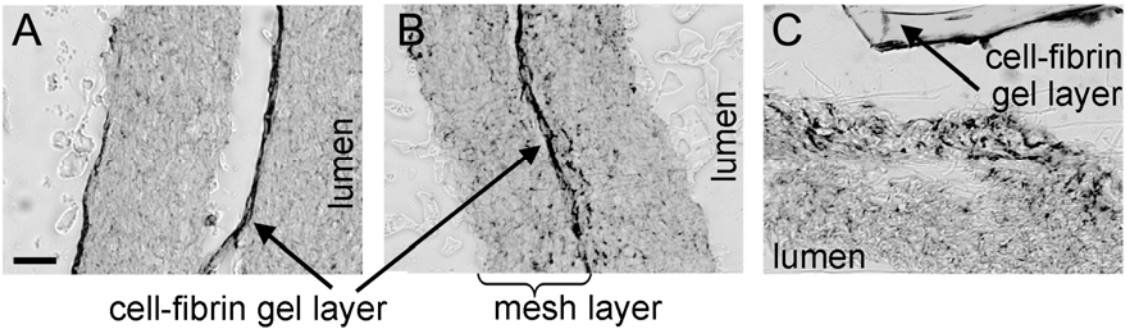

Figure 7. SM22α staining as an indicator of cell migration into the mesh layers of PEG-fibrin mesh hybrid scaffolds. (A) A representative image of an SM22α-stained, transverse section through a composite scaffold at the time of composite construct fabrication. (B) The average observed extent of SM22α staining within a transverse section of a static, hydrogel-mesh composite construct following 16 days of total culture. (C) The average observed extent of SM22α staining within a transverse section of a dynamic, hydrogel-mesh composite construct following 16 days of total culture. The images reflect the fact that cryosections of the composite constructs failed to adhere to charged slides. The constructs therefore experienced significant mechanical stress during the immunostaining process which tended to result in the separation of individual construct layers. The scale bar in (A) applies to all images and represents 25 μm. The "lumen" label associated with each image is intended to give orientation information and is not intended to imply that that particular surface contacted the lumen.

ELISA results supported the similar degree of per cell SM22α expression in static and dynamic composite constructs that was indicated by immunostaining (**Figure 8**). In addition, ELISA measures of the average per cell calponin h1 levels in the static and dynamic hybrid grafts could not be distinguished. Regarding ECM protein production, ELISA data indicated that collagen I, collagen III, and elastin were able to accumulate within both the static and mechanically-conditioned composite scaffolds (**Figure 8**). Immunohistological evaluation of collagens I and III supported these ELISA results and demonstrated that these newly synthesized ECM proteins were able to deposit within the mesh structure (**Figure 9**).

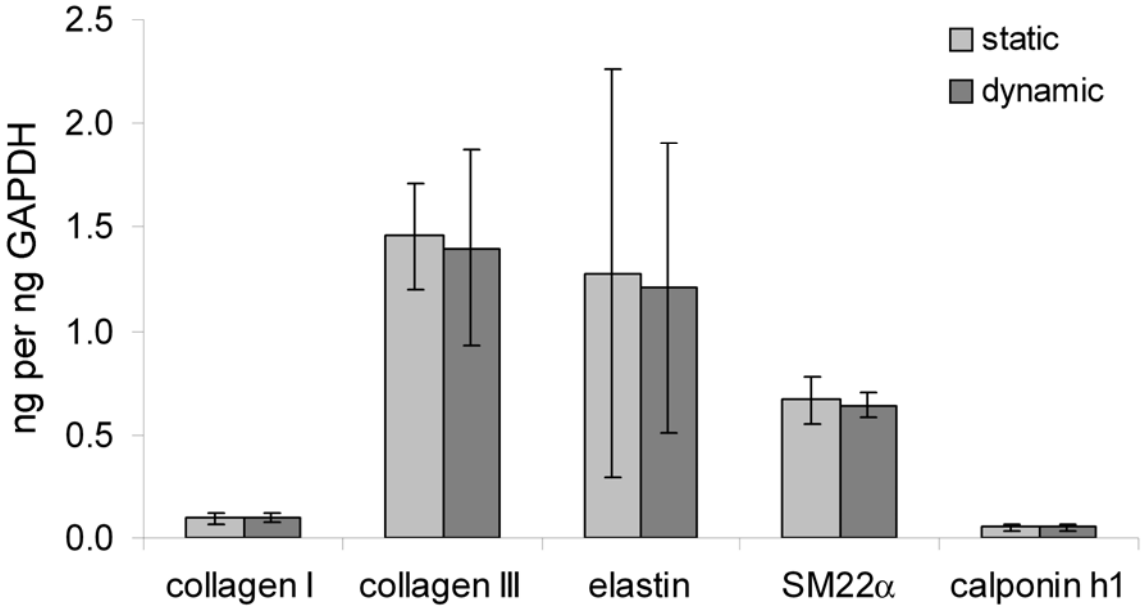

Figure 8. ELISA results for collagen I, collagen III, elastin, SM22α, and calponin h1 normalized to housekeeping protein GAPDH.

2.4 Discussion

The aim of the current study was to investigate the potential of hydrogel-electrospun mesh scaffolds for CABG applications. These composite scaffolds were generated by rolling a PEUUR electrospun mesh around an inner mandrel and subsequently bonding the juxtaposed mesh layers together using a fibrin-based hydrogel matrix. The underlying hypothesis of this work was that these composite scaffolds would exhibit key features of the individual mechanical response of each component, with the "low stiffness" behavior of the hybrid constructs being dominated by the hydrogel and the "higher stiffness" behavior being dominated by the mesh. These hybrid scaffolds would thereby more closely approach the biphasic mechanical response of native vessels than would electrospun mesh alone. Consistent with this hypothesis, circumferential mechanical testing of PEG-fibrin-mesh constructs revealed a "J-shaped" stress-strain curve similar to that of native human coronary artery which was not achieved by electrospun mesh-only grafts.

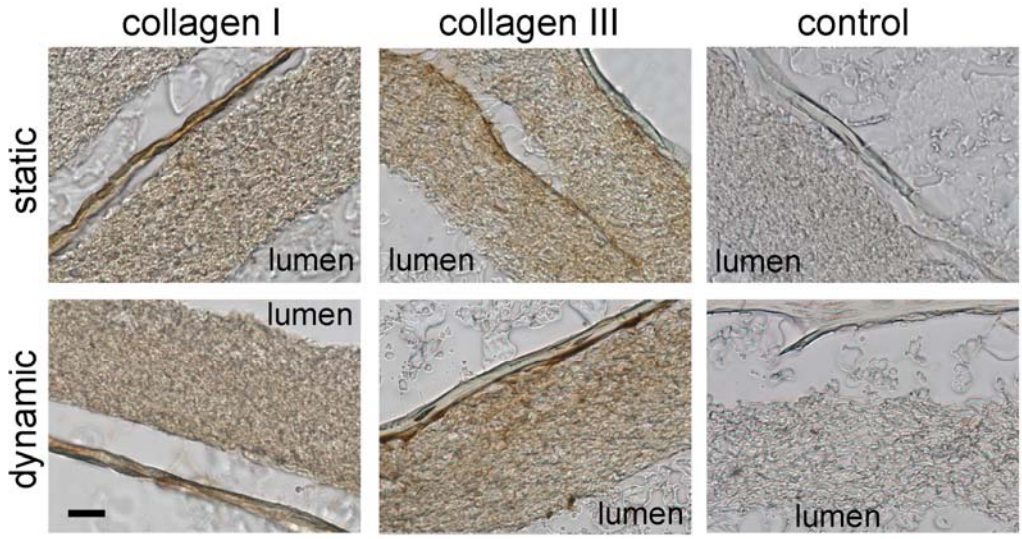

Figure 9. Representative images of transverse sections through statically- and dynamically-cultured composite constructs following immunostaining for collagen I and collagen III. Images of corresponding negative control sections (which received control IgG serum in place of primary antibody) are included for comparison. Observed detachment between adjacent mesh layers reflects the fact that cryosections of the composite constructs failed to adhere to charged slides. The constructs therefore experienced significant mechanical stress during the immunostaining process which tended to result in the separation of individual construct layers. The scale bar applies to all images and represents 25 μm. The "lumen" label associated with each image is intended to give orientation information and is not intended to imply that that particular surface contacted the lumen.

In addition, the hybrid scaffolds appeared to retain the high suture retention strengths typical of electrospun mesh, displaying an average suture retention strength similar to that reported for mammary artery (~1 N) (23), a preferred coronary artery graft material (5). Thus, these results indicate that the hydrogel-mesh composite scaffolds have suture retention strengths sufficient for implantation at the time of preparation. The average tangential modulus of freshly prepared composite constructs at physiological pressures exceeded the target 0.20-0.40 MPa range associated with coronary artery by ~20% (42). However, these hybrid scaffolds more closely mimic the tangential modulus

range of native coronary artery than do human saphenous vein grafts, another preferred coronary artery graft (5). Specifically, human saphenous vein displays a tangential modulus of ~2 MPa under similar testing conditions (23). In terms of tensile strength, the 24 h hybrid scaffolds exhibited an average circumferential UTS of 0.32 MPa, which is consistent with the ~0.37 MPa UTS measured for vertebral artery by circumferential ring tests (35). However, this average hybrid scaffold UTS is significantly lower than the ~3.7 MPa circumferential UTS reported for human saphenous vein (23). Additional tuning of the material properties of the individual construct components and their cohesion may further improve the correspondence between the initial composite graft tangential modulus and UTS values and the respective target values. Alternatively, an "outer" sleeve could be incorporated into the construct design to increase construct UTS decoupled from vessel regional stiffness considerations (43).

The average endpoint tangential modulus of both the static and dynamic composite constructs remained similar to the 24 h values. Moreover, static constructs maintained the observed 24 h circumferential UTS values following prolonged culture. However, the inter-sample variation in tangential modulus and UTS within both the statically-cultured and the mechanically-conditioned treatment groups increased notably with time in culture. For instance, the standard error of the mean for the 24 h tangential modulus measures was ~6 % of the average value, whereas the standard error of the mean for the tangential modulus measures of the endpoint dynamic constructs was ~26 % of the average value. In addition, extended cyclic distension was associated with a significant decrease in composite scaffold UTS relative to initial graft properties. Based

on visual comparison of the endpoint static and dynamic constructs prior to mechanical testing, the tangential modulus and UTS of the composite scaffolds appeared to be highly correlated with the integrity of the fibrin hydrogel bond with adjacent mesh layers. For static constructs, the increase in inter-sample variation in modulus and UTS relative to that of the 24 h constructs was therefore likely due, in part, to the degradation of the fibrin gel and/or mesh components and the associated reduction in gel-mesh bond integrity. In the mechanically-conditioned constructs, mechanical shearing between the electrospun mesh and hydrogel layers induced by repeated construct distension may represent an additional mechanism for reduction in the integrity of the fibrin-mesh bond. Increased cell matrix metalloproteinase expression upon cyclic distension may also be involved in the observed difference in UTS between static and dynamic hybrid grafts (44). It can be hypothesized that approaches to increase the strength of the inter-mesh adhesive bond, such as pre-treating the mesh to increase its hydrophilicity or soaking the mesh in fibrinogen solution prior to rolling, would increase long-term construct mechanical integrity.

Although increasing the hybrid scaffold inter-layer cohesion can be expected to prolong initial construct integrity, the maintenance of appropriate graft mechanical properties over the long-term requires cell infiltration throughout the construct layers and sufficient associated neomatrix accumulation. Present results suggested that cells were able to migrate through the mesh layers of the composite scaffolds. In addition, mechanical conditioning appeared to enhance cell motility, either by forcing repeated microstructural changes in the mesh and/or by inducing alterations in cell phenotype

(45). Similarly, ELISA and immunohistological data indicated that the composite scaffolds were able to support ECM accumulation. Although no differences in the levels of collagen type I, collagen type III or elastin were observed between static and dynamic constructs in the present study, this result may be due to the relatively low average strains (~2.5%, as estimated by the Bernoulli equation) experienced by the dynamic constructs. Specifically, previous literature indicates that strains exceeding 5% are generally necessary for alterations in SMC ECM production and phenotypic markers to be observed *in vitro* (46). Decreasing mesh thickness or fiber density (47) and/or employing vacuum and/or centrifugal seeding methods (48) may allow for increased cell penetration into the mesh layers, and therefore more even neomatrix distribution within the composite scaffolds.

Cumulatively, the present results suggest that hydrogel-electrospun mesh composites warrant further investigation as scaffolds for arterial tissue engineering. In addition, these hybrid scaffolds may have potential applicability in the regeneration of other soft tissues with biphasic loading responses, such as ligament. Although the PEUUR2000 formulation used herein has not been demonstrated to have an optimal degradation rate for vascular applications, the broad tunability of the elastic modulus, UTS, and degradation rate of polyurethane-based elastomers can be exploited to identify formulations which display desired mechanical properties as well as appropriate degradation rates. Our future CABG hydrogel-mesh composite studies will also focus on modifying the fibrin gel composition and composite construct fabrication methods to improve inter-layer cohesion.

CHAPTER III

REGULATION OF SMOOTH MUSCLE PHENOTYPE BY EXTRACELLULAR MATRIX PROTEIN IDENTITY

3.1 Introduction

Blood vessel replacements are often necessary in the treatment of advanced atherosclerosis, aneurismal and peripheral vascular disease, etc. In the US alone, more than 500,000 coronary artery bypass procedures are performed annually. Tissue engineering represents a potential means to construct functional grafts when compared to the limited availability of autologous saphenous veins and relatively poor elasticity and low compliance of synthetic materials (mainly Dacron and polytetrafluoroethylene) (6). To improve the designing of tissue engineering vascular grafts, a great challenge is to obtain a well organized and functional medial layer which is mainly comprised of mature SMCs. The utilization of mesenchymal progenitor cells with given differentiation conditions to obtain SMC has become one of the promising ways to overcome the challenge (49, 50). In order to differentiate the mesenchymal progenitor cells towards SMC, soluble growth factors such as transforming growth factor-beta1 (TGFβ1), ascorbic acid, and insulin are widely used (51-53). Although the inductions of these growth factors are very efficient and stable *in vitro*, there are still some drawbacks of them especially in tissue engineering applications. The growth factors are too expensive to be used in large scale applications, and the growth factors have undesired effects on neighboring tissue. Also, soluble growth factors are difficult to control in tissue

engineering constructs. Recently A. J. Engler et al. showed that the matrix stiffness can direct stem cell lineage specification with similar effect as growth factors and furthermore soluble induction factors tend to be less selective than matrix stiffness in driving specification, and cannot reprogram MSCs that are pre-committed for weeks on a given matrix (54). And G.E Plopper's group has shown that only the ECM can be sufficient to induce progenitor cells to osteoblasts (55, 56). Moreover, C. Chen's group also showed the influence of ECM on stem cell fate through physical interactions with cells such as the control of cell geometry, ECM geometry/topography, ECM mechanical properties (57). From all the previous reports, it is still unclear which properties of the ECM are most critical in terms of determining the cell fate of progenitor cells. In this project, we will examine the bioactivity identity of given ECM components to verify if it is the dominant stimuli in cell-material interactions.

In the process of vasculogenesis, it is understood that the assembly of the vessel wall from its cellular and ECM components is a critical process in the development and maturation of the vertebrate vascular system (58). Previous literature has demonstrated that fibronectin and laminin play significant roles in this process (58, 59). Fibronectin plays a role in the early migratory events of vessel wall development and correlates the production of laminin, contained in the basement membrane, to vessel wall maturation (58, 60). The absence of fibronectin and collagen type I will cause the disruption of endothelial cell tubes (61). During vasculogenesis, the dynamic composition of the ECM also brings attention to how the ECM functions in mural cells differentiation. The transition of ECM composition from fibronectin and collagen type I to laminin and

collagen type IV when the mural cells start differentiation could imply that these molecules may have some impact on inducing and/or maintaining the SMC phenotypes (62). Recently it has been shown that when the mural cells undergo differentiation, fibrin can also be found around the leaky vessel precursors, which gave rise to the hypothesis that fibrin may be involved in SMC differentiation process. Also, it has been demonstrated that adult human bone marrow progenitor cells can induce a dynamic self organization process to create vascular structures within 3D fibrin matrices (63). In this project we chose collagen type IV, fibrinogen, fibronectin, laminin as the biochemical stimuli and RGDS as the control.

In order to study the differentiation of the progenitor cells, we choose mouse mesenchymal smooth muscle progenitor 10T½ cells, which are well characterized multipotent embryonic fibroblasts. 10T½ cells are very sensitive to both the post confluence inhibition of cell division, and the microenvironment, which will induce this mesenchymal cell line to differentiate into different cell types, e.g. smooth muscle cell (64), cartilage lineage (65), etc. Unlike the human mesenchymal stem cells, which are very unstable in different culture systems and vary from the different donors, 10T½ cells give more reliable and reproducible response to the experimental microenvironment. In the past few decades, the 10T½ cells have been one of the most studied systems for the investigation of smooth muscle cell differentiation and the associated cell signaling pathway. Sato and his colleagues (66) demonstrated the activation mechanism of TGFβ1-induced smooth muscle cell-genes in 10T½ cells. Wang and his colleagues (67) investigated the transactivation of cardiogenic genes in 10T½ fibroblasts. S.C Lien et al

(64) have shown that Phosphatidylinositol 3-kinase/Akt pathway was involved in TGFβ1-induced phenotypic modulation of 10T½ cells to smooth muscle cells. However, the reports on the 10T½ cells differentiation in three dimension culture system are limited. Recently the importance of studying cell behavior in three dimension culture has been emphasized because essential cellular functions that are present in tissues are missed by 'petri dish'-based cell cultures. Two dimensional culture limits the potential to predict cellular responses of real organisms *in vitro* (68). This project aims to give us insight into the differentiation of progenitor cells in three dimension culture systems.

Over the past three decades, a number of hydrogels have been developed, differing in structure, composition, and properties. Due to the hydrophilic but crosslinked structure, hydrogels can swell large quantities of water without the dissolution of the polymer, thus giving them physical characteristics similar to soft tissues (69).

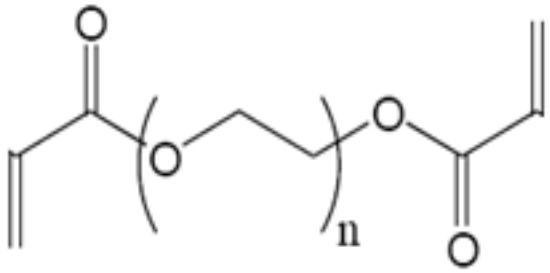

Figure 10. Molecular structure of poly(ethylene glycol) diacrylate (PEGDA).

Poly(ethylene glycol) (PEG) hydrogel is one of the most common used biomaterials because of its excellent biocompatibility, non-biofouling and easy fabrication. In recent years, many researchers have applied PEG hydrogel to diverse

aspects in tissue engineering including drug delivery (70), tissue restoration (6, 71-73), and cell-materials interactions (74, 75).

In the present work, PEGDA based hydrogel was functionalized by ECM proteins, such as fibronectin, fibrinogen, laminin and collagen type IV to create a three dimensional construct with encapsulated smooth muscle precursor cells 10T½ cells to study the impact of ECM protein identity on regulation of smooth muscle phenotype.

3.2 Materials and Methods

3.2.1 Poly(ethylene glycol) (PEG) Hydrogel Preparation and Cell Encapsulation

Poly(ethylene glycol) (PEG) (MW10000, Fluka) was diacylated using the common method described previously (75) by combining 0.1 mmol/ml dry PEG, 0.4 mmol/ml acryloyl chloride, and 0.2 mmol/ml triethylamine in anhydrous dichloromethane (DCM) and stirring under argon overnight. The resulting solution was washed with 2 M K_2CO_3 and separated into aqueous and DCM phases to remove HCl. The DCM phase was subsequently dried with anhydrous $MgSO_4$, and PEGDA was precipitated in diethyl ether, filtered, and dried under vacuum. The molecular structure of PEGDA is shown in **Figure 10**.

ECM molecules, such as the fibronectin (MP Biomedicals) , fibrinogen (MP Biomedicals), collagen type IV(Sigma) and laminin (Sigma), were chemically linked to the ACRL-PEG-NHS (MW 3400, Nektar) according to the protocol described previously (76). The reaction between the NHS and the primary amine in the proteins is

shown in **Figure 11.** Arg-Gly-Asp-Ser (RGDS), the cell binding peptide was also PEGylated as control.

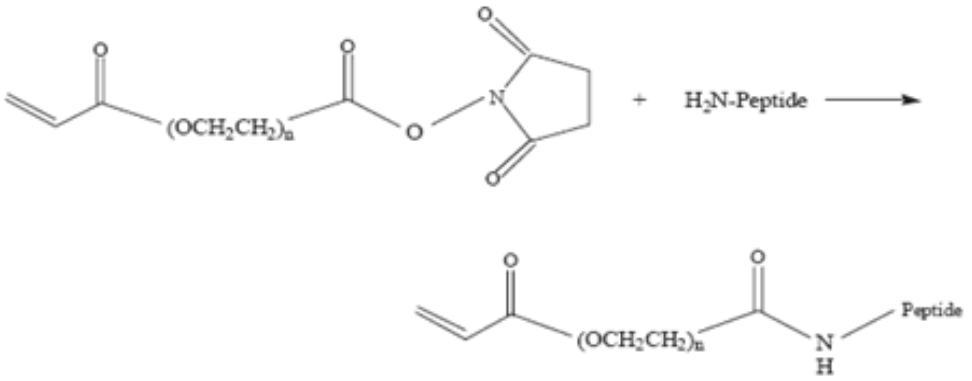

Figure 11. Incorporation of peptides and/or proteins containing α-amine to ACRY-PEG-NHS. (69, 77)

10T½ cells (Passage 3~4) were suspended in the precursor solution containing 10% of 10k diacrylated PEG (PEGDA), 3mg/ml acetophenone and 0.5mg/ml ACRL-PEG-Proteins in HEPES buffered saline (HBS; 10 mM HEPES, 100 mM NaCl, pH 7.4), at a cell density of 1 million/ml. Then the precursor solution was poured into glass cassette with 0.5 mm spacers and UV irradiated (UVP model B-100SP, 10mW/cm^2, 365 nm) for 3 minutes on each side. The cured hydrogels with encapsulated cells were removed from the cassettes and then immersed in phosphate buffered saline (PBS, pH7.4) plus 100 IU/mL penicillin, 100 µg/mL streptomycin and 250ng/mL Amphotericin B (MP Biomedicals). The hydrogels were then transferred to the Dulbecco's Modified Eagle Medium (DMEM, Mediatech) supplemented with 10% heat treated fetal bovine serum (dFBS, HyClone) and 100 IU/mL penicillin, 100 µg/mL streptomycin and placed

in the incubator with 5% CO_2. The media was changed every other day. Samples were taken at 1 week time point.

3.2.2 Cell Chip

Agilent 2100 analyzer with the Cell Fluorescence LabChip®Kit were used to characterize the cell phenotype. 10T½ Cells (approximately 0.2million per staining) were collected and washed with cold D-PBS once and resuspended in staining buffer (PBS supplemented with 1% BSA) to reach 2million/ml. 2uM of the calcein was used to stain the live cells for 30mins at room temperature in dark. The cells were washed twice before adding the antibody. Staining was performed by adding to the cells 1ug of the primary antibody (SCBT unless stated specifically) and appropriate isotype controls (SCBT, Jackson Imunoresearch) diluted in 100ul of the staining buffer. All samples were incubated on ice for 30mins. Fluorescence-labeled secondary antibodies were used to label the cells with 1:50 dilution in staining buffer and the incubation was done on ice for 30mins avoiding light. Labeled cells were spun down and resuspended in 30ul of the cell buffer and 10ul of the sample were loaded to the cell chip according to the manufacturer. Antibody used: Anti-CD105 (MJ7/18), Anti-CD44 (1M7), Anti-CD34 (MEC14.7), Anti-CD45 (30-F11), Anti-mouse-IgG-633 (Invitrogen), Anti-rat-IgG-Dylight 649 (Jackson Immunoresearch).

3.2.3 Quantitative Protein Expression Analyses

Sample proteins were isolated using a modification of a procedure validated by Hummon *et al* (78). In brief, the phenol-chloroform phase resulting from Trizol-based RNA extraction was mixed with ethanol to precipitate residual DNA. The resulting

phenol-ethanol phases for all constructs in a given ECM component group (e.g., all Fibronectin constructs) were combined and transferred to a 3.4 kDa SnakeSkin dialysis membrane (Pierce). The solutions were dialyzed for ~60 h at 4 °C against an aqueous solution of 0.1% sodium dodecyl sulfate (SDS), with buffer exchange every ~18-20 h. By the end of third 18-20 h dialysis period, the samples had partitioned into three phases: (1) a supernatant, (2) a globular mass, and (3) a colorless, viscous liquid. The globular mass, containing the bulk of sample proteins, was resuspended in PBS containing 0.5% SDS and 1% Triton X-100.

Competitive Enzyme-linked immunosorbent assay (cELISA) was used to analyze the protein expression quantitatively. In brief, approximately 200ng of the given peptide was coated in the EIA high binding plate (Corning) at 4°C overnight. The second day, standards and the samples were diluted in PBS containing 0.05% Tween20 (Sigma) and 3% bovine serum album (BSA) (Fisher) and competition between the free antigen in solution and the antigen on the coated well was formed by mixing the samples and/or the standards with the primary antibody solution in given dilution at room temperature for 1 hour before loading the mixture to the coated wells for another 1 hour. The bound primary antibody was detected by applying donkey anti-mouse/anti-goat/anti-rabbit-IgG-HRP (Jackson Immunoresearch), which is also diluted in 3% BSA in PBST, followed by application of 2,2′-Azino-bis(3-ethylbenzothiazoline-6-sulfonic acid) (ABTS, sigma). The color development was monitored with a microplate reader at the wavelength of 410. All antibodies and peptides used were from Santa Cruz unless described specifically.

3.2.4 Statistical Analyses

All data are reported as mean ± standard error of the mean. Comparisons among hydrogel treatment groups were conducted using ANOVA and Tukey's post-hoc test (SPSS software), $p < 0.05$.

3.3 Results

3.3.1 Characterization of the Initial Phenotype of 10T½ Cells

Since the 10T½ cells have the potential to undergo differentiation into different cell lineages, such as smooth muscle cells (64), chondrocytes, osteoblasts (65, 79) and etc, cell characterization at the initial status needs to be performed to confirm that the cells are undifferentiated. A cell fluid-based microchip was used to analyze the cell phenotype using 2100 bioanalyzer (Agilent) with similar principle of flow cytometry (80). To verify the phenotype of 10T½ cells at the start point, surface markers such as CD105, CD34, CD44, and CD45 were tested before the cell encapsulation. As is shown in **Figure 12 (A-D)**, the 10T½ cells showed positive staining of CD105 and CD44, but the cells didn't express detectable level of CD34 and CD45, which demonstrated that the cells were not differentiated according to previous literature (81, 82).

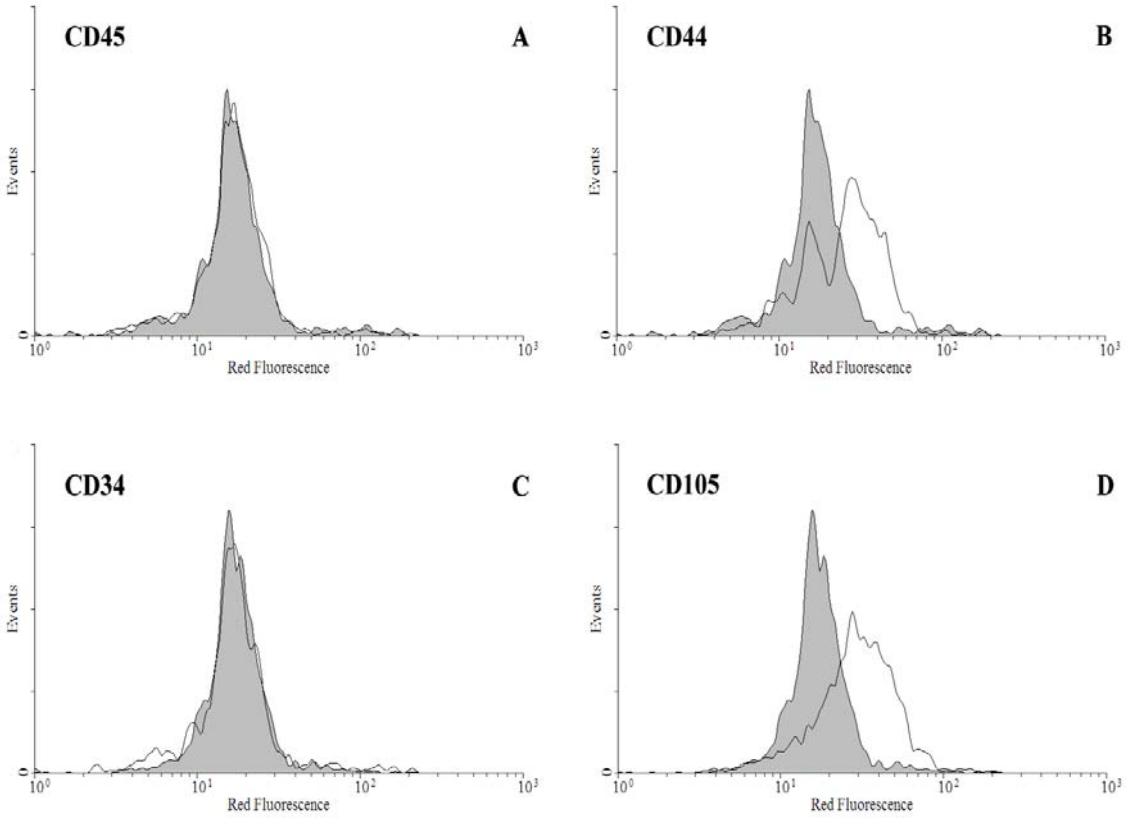

Figure 12. Immunophenotyping of 10T½ cells by cell chip based flow cytometry. Single parameter histograms showed the relative fluoresecence intensity of staining and the cell counts. Isotype controls were included to show the background fluorescence, as is shown in shaded peaks. The open peaks represented the common MSC markers: CD45, CD44, CD45, CD105. The 10T½ cells were positive for CD44, and CD105, but negative for CD34 and CD45. Gate was set up according to calcein stain for live cells.

3.3.2 Assessments of Expression of Differentiation Markers

To assess the 10T½ cells differentiation under the impact of the different ECM proteins, ELISA was performed to monitor the differentiation markers of different cell lineages, namely, SM22α for SMCs, collagen type II for chondrocytes, osteocalcin for osteoblasts, and A-FABP for adipocytes. After 7 days of culture, it was demonstrated that within the protein concentration range used in this study, the impact of ECM protein identity was relatively weak on mouse smooth muscle precursor cell differentiation (**Figure 13**). Fibrinogen, fibronectin, collagen type IV, laminin showed no preference in myogenesis in terms of SM22α expression relative to the RGDS control (**Figure 13A**). Collagen type II expression also showed great consistency across all the formulations (**Figure 13B**), suggesting that chondrogenesis was not altered by these ECM proteins alone to a detectable level. However, A-FABP and osteocalcin expression showed weak difference among groups. In the fibrinogen and fibronectin containing hydrogels, late-term adipogenic marker A-FABP was reduced relative to collagen IV gels and RGDS control gels, and compared to laminin functionalized hydrogel, the A-FABP expression in fibrinogen gel was significantly decreased ($p=0.033$) (**Figure 13C**). In fibronectin gels, osteocalcin expression was relatively lower than other gels and moreover, the difference between fibronectin gels and laminin gels were statistically significant ($p=0.014$) (**Figure 13D**). Although there are some significant differences in differentiation marker expressions under the impact from ECM proteins, the difference was not strong enough to be dominant.

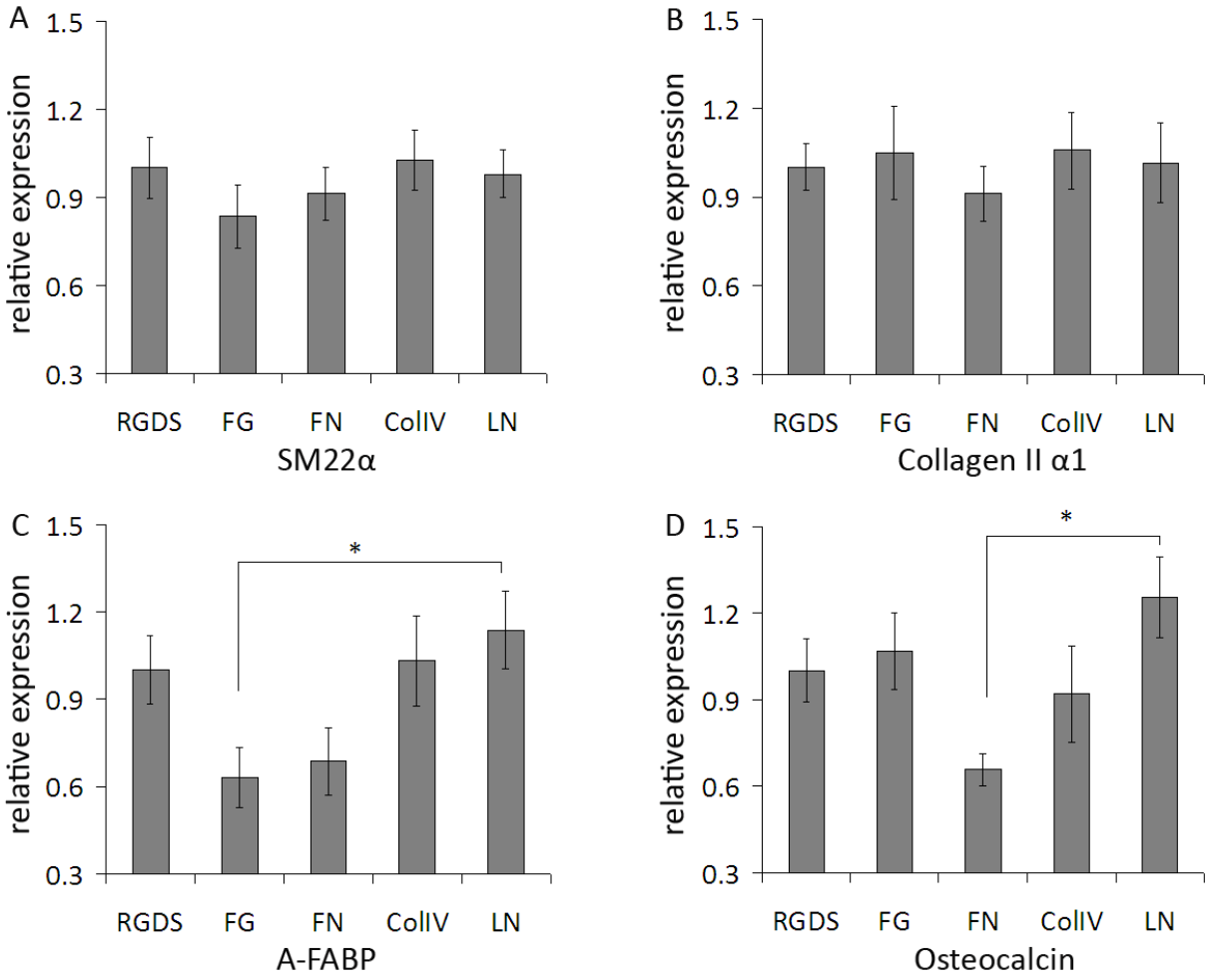

Figure 13. Assessment of 10T½ cells differentiation under the stimuli from different ECM proteins after 7 days by comparison of relative expression of the differentiation markers for different lineages. Namely, SM22α for SMCs, collagen type II for chondrocytes, osteocalcin for osteoblasts, and A-FABP for adipocytes. Asterisk (*) indicates significant difference, $p<0.05$. All data of fibrinogen (FG), fibronectin (FN), collagen type IV (ColIV), laminin (LN) have been normalized to the corresponding RGDS control.

3.3.3 Analysis of Integrin Profile

Integrins are the primary mediators of cell-ECM interactions and this family of proteins exert profound control over cells (83). The integrins are necessary in mediating

both mechanical and chemical signals from the ECM. A growing body of literature demonstrated that integrins play important roles in cell proliferation and cell differentiation (84). In the present work, we analyzed the expression profile of integrin α1, integrinα3, integrin α5, and integrin α6, because all of them are important in cell-ECM interactions, and have specificity over different ECM proteins. For example, integrin α1 is specific for collagen type I, collagen type IV and laminin; integrin α3 is specific for laminin, collagen and fibronectin, while integrin α5 only recognize fibronectin; and integrin α6 serves as a specific laminin receptor (83).

Fibronectin, fibrinogen, collagen type IV and laminin seem to have limited potency to regulate expression of integrin α1 (**Figure 14A**), integrin α3 (**Figure 14B**) integrin α5 (**Figure 14C**), and integrin α6 (**Figure 14D**), since no significant difference in relative expression has been detected across the hydrogel formulations. However, integrin expression can be correlated to the smooth muscle phenotypic modulation, and in particular, integrin α1 is transcriptionally regulated in a SMC phenotype-dependent manner (85). As is shown in **Figure 13A** and Figure **14A**, the SM22α expression shared great consistency with integrin α1 expression, which further demonstrated the limited influence of ECM protein on SMC phenotype. Although the expression level of integrin α3 was not altered within different ECM functionalized gels, the expression levels were significantly elevated compared to cell cultured in poly styrene flask (RGDS $p=0.049$, LN $p=0.007$). This might be because of the different mechanical property between hydrogel and culture flask, and also due to the difference between cellular responses in 2D and 3D cell culture systems.

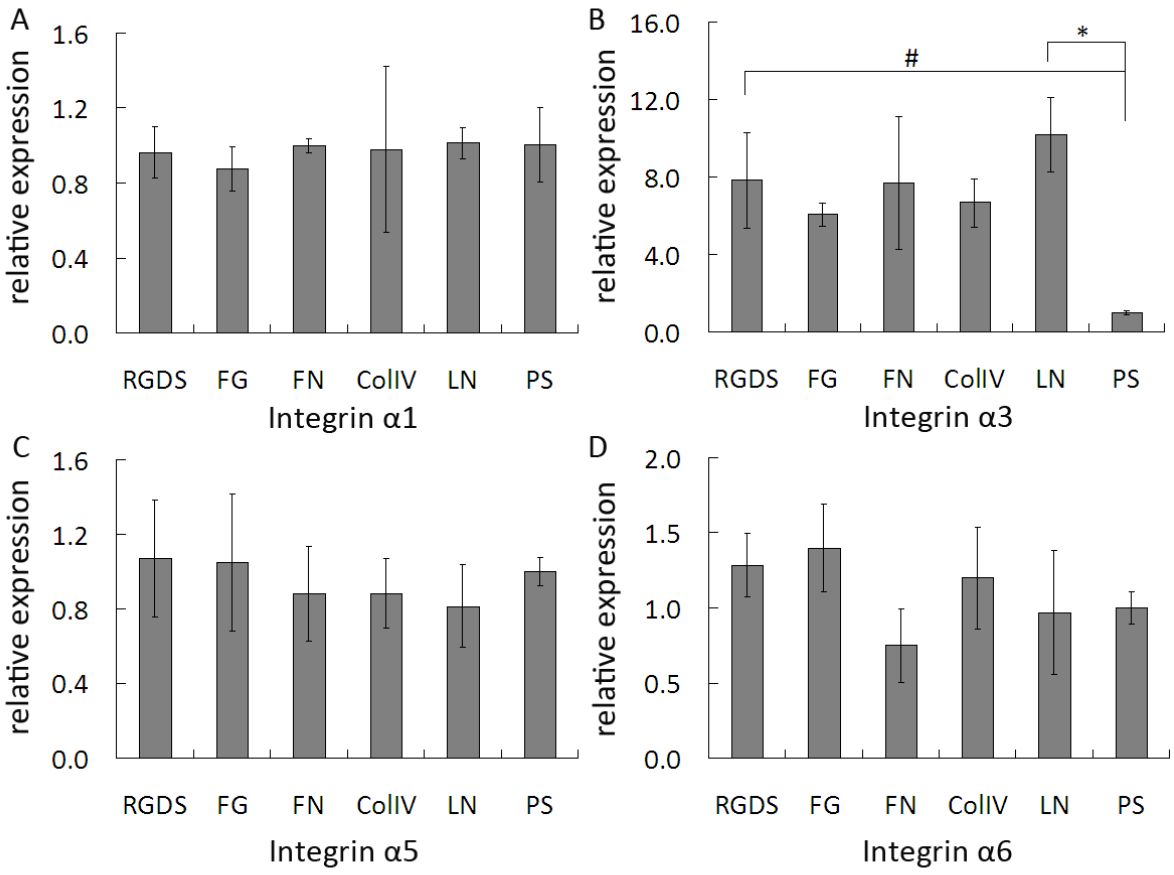

Figure 14. Integrin profiling of the encapsulated 10T½ cells after 7 days. Relative expression of integrin α1, α3, α5 and α6 were measured and compared across formulations. Data from the encapsulated cells have been normalized to corresponding data of 10T½ cells cultured in poly styrene culture flask (PS). Asterisk (*) indicates significant difference, $p<0.05$, between PS sample and LN sample; # significantly different between PS sample and RGDS sample, $p<0.05$.

3.3.4 Evaluation of Cell Signaling Activation

From the ELISA results of differentiation markers and integrins, the ECM protein identity showed limited impact on regulating the expression of differentiation

markers in 10T½ cells. To further study the interactions between smooth muscle precursor cells and ECM proteins, the activation of important cell signaling switches was investigated. MAP (mitogen-activated protein) kinases play a significant role in cell adhesion and spreading, cell differentiation and apoptosis (86). The interactions of integrins and MAP kinases have been well studied in an extensive body of literature (87, 88).

Given the important and ubiquitous involvement of MAP kinases in the regulation of gene expression and cellular differentiation, we tested the activation of two MAP kinases, JNK, and ERK. **Figure 15** shows that the activation of ERK1/2 and JNK was relatively consistent across the formulations. Although the activation of ERK1/2 and JNK showed limited difference among the groups, they showed very similar trend to some of the differentiation marker expression, for example, pERK1/2 and A-FABP, which is consistent with the correlation between the modulation of adipogenic phenotype and the MEK/ERK signaling cascades (89).

3.4 Discussion

The aim of this present study was to examine the impact of ECM protein identity on regulation of smooth muscle phenotype. Smooth muscle precursor cell, 10T½ cells were encapsulated into ECM protein functionalized hydrogel and cultured for 7 days with normal growth media without additional growth factor. The hydrogels have the appropriate mechanical property for smooth muscle cell differentiation (54). But no significant impact of ECM protein identity on smooth muscle differentiation has been

detected within our experiment conditions. We have examined the expression of differentiation markers, activation of the cell signaling switches, and expression of the

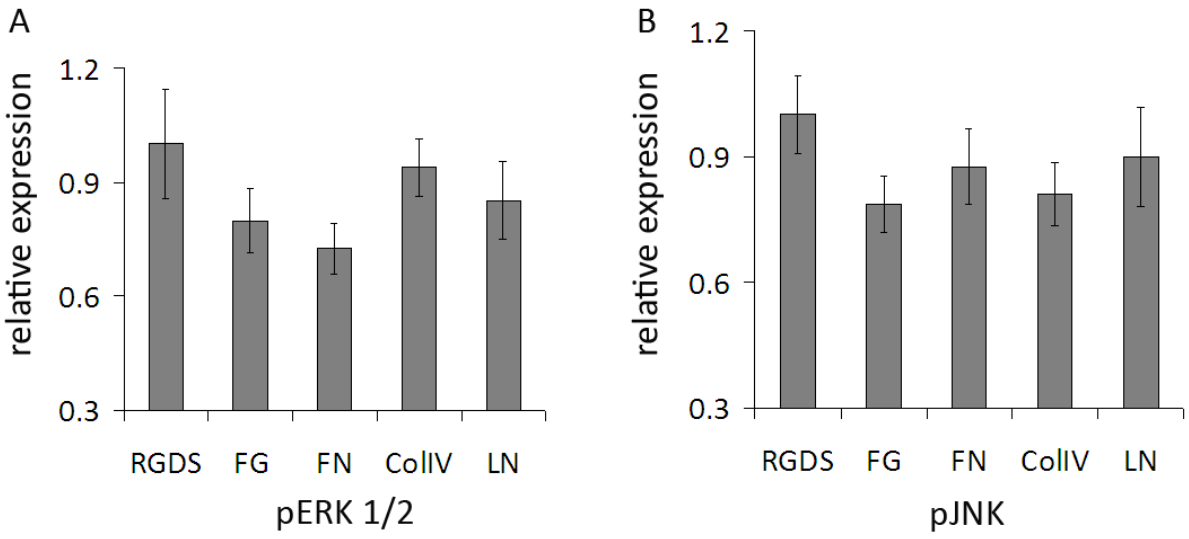

Figure 15. Evaluation of MAP kinases activation under the stimuli from different ECM proteins after 7 days by comparison of relative levels of the phosphorylated ERK1/2 and JNK. Anti-p-ERK 1/2 (Thr 202/Tyr 204), and anti-p-JNK (Thr 183/Tyr 185) antidbodies were used in the ELISA. Data of RGDS control was used for normalization.

surface adhesion receptors. Surprisingly to us, the impact of the ECM proteins identity was quite limited in all three aspects. To support our conclusion, a previous work done by Gong and Niklason(90) also showed that SMC early differentiation marker smooth muscle α-actin was not altered in human mesenchymal stem cells cultured on collagen type IV, fibronectin and laminin matrix, while the mid-term SMC marker calponin stayed the same on collagen and fibronectin but slightly decreased on laminin matrix. In contrast to our finding, Hedin et al indicated that fibronectin can promote a synthetic

phenotype while, laminin and collagen type IV helps maintain contractile phenotype of arterial SMCs (91), this could be due to the difference between the nature of mature SMCs and smooth muscle progenitor cells. Moreover, their work was done in petri-dish based 2D cell culture system, while our research focused on 3D hydrogel system, which could be a superior mimic of nature microenvironment (92).

It seems the ECM protein identity is a weak variable in driving progenitor cell differentiation at least at the studied concentration, although we found a promising repression of osteogenesis and adipogenesis by fibronectin content (**Figure 13C, D**). The limitation may come from the limited concentration range used in the study, and the fact that vasculogenesis is a sequence, but we are not following the sequence, as we only examine individual components.

To our knowledge, this is the first time that phenotypic regulation of smooth muscle progenitor cells by ECM protein identity has been studied in a controlled manner in 3D hydrogel system. By introducing PEGDA hydrogel system, we could rule out the variation of mechanical property across formulations because the modulus and mesh size were determined mainly by the PEGDA content. Utilization of 3D culture system helps mimic the real micro environment for tissue growth and induce more native cellular behavior than the typical 2D culture (92). Although we didn't observe a strong impact of ECM protein on smooth muscle differentiation, the platform we designed for this study could still be expanded with other biochemical stimuli to investigate cellular behaviors in three-dimensional scaffolds.

CHAPTER IV

REGULATION OF SMOOTH MUSCLE PHENOTYPE BY GLYCOSAMINOGLYCAN IDENTITY*

4.1 Introduction

As the predominant cell type found in the arterial wall, smooth muscle cells (SMCs) are believed to play essential roles in the structural and functional integrity of the vessel (93). In contrast to most cell types that experience terminal differentiation, SMCs retain remarkable plasticity in phenotypic modulation in response to local microenvironmental stimuli (94). An extensive body of literature dictated that SMC phenotypic regulation showed great influence in arterial injury and cardiovascular disease. For example, medial SMCs expressed osteogenic and chondrogenic marker proteins, such as alkaline phosphatase, type II collagen has been reported in calcified blood vessels (93, 95, 96). The conversion of SMCs from a contractile phenotype to a synthetic phenotype has also been reported in atherosclerosis (97). To improve our design of TEVG and the associated biomaterials, a comprehensive understanding of cell material interactions in terms of inducing appropriate SMC phenotype while repressing the undesired diseased phenotype would provide important clues.

Coronary artery disease is a leading cause of death in the United States (98) and

---

*Reprinted with permission from "Regulation of Smooth Muscle Cell Phenotype by Glycosaminoglycan Identity" by X. Qu, A.C Jimenez-Vergara, D.J. Munoz-Pinto, D. Ortiz, R.E. McMahon, D Cristancho, S. Becerra-Bayona, V. Guiza-Arguello, K.J. Grande-Allen, M.S. Hahn, 2011. *Acta Biomaterialia*, 7(3), 1031-1039, Copyright [2010] by Acta Materialia Inc. Published by Elsevier Ltd.

develops when excess cellular and ECM components build up in the coronary arteries through the process of atherosclerosis (10, 99, 100). Until recently, it was generally believed that the extracellular lipids associated with early atherosclerosis originated from dead foam cells derived from invading macrophages. However, it is now recognized that this early accumulation of lipids precedes macrophage infiltration and instead arises primarily from enhanced lipoprotein retention by the ECM of the arterial intima (10, 99, 100). In fact, recent studies indicate that ionic interactions between the negatively-charged glycosaminoglycan (GAG) side chains of intimal proteoglycans (PGs) and the positively-charged apolipoprotein residues of low density lipoproteins (LDL) are critical to early atherosclerotic lipid retention (101-103).

As arterial LDL loading increases in atherogenesis, macrophages and smooth muscle cells (SMCs) increasingly infiltrate into the intima, followed by the appearance of foam cells (10). Although foam cells were long considered to arise exclusively from macrophages, it is now known that SMCs form a significant portion of the foam cell population (104, 105). The transition of SMCs to foam cells is marked by the acquisition of macrophage-like behaviors, such as scavenger-receptor uptake of LDL (106, 107), and/or by the acquisition of adipocyte-like properties, including expression of adipocyte fatty acid-binding protein (A-FABP) (105). Although it is recognized that GAG retention of lipoproteins is a key event in SMC foam cell formation (10), the extent to which specific GAG types contribute to this process is relatively poorly understood. Thus, the present work was designed to explore the impact of GAG identity on SMC phenotype using a scaffold environment intended to be mimetic of early atherosclerosis.

Specifically, the influence of chondroitin sulfate C (CSC), dermatan sulfate (DS), and an intermediate molecular weight hyaluronan (HA_{IMW}, ~400 kDa), were examined, as the levels and/or distribution of each of these GAG types are altered in early atherosclerosis (10, 108-113).

To generate culture conditions mimetic of early atherosclerosis, a poly(ethylene glycol) diacrylate (PEGDA) hydrogel was selected as the base scaffold into which desired GAG signals were conjugated. PEGDA gels have several properties which make them appropriate for the present studies. First, pure PEGDA hydrogels function as biological "blank slates" in that they do not significantly adsorb bioactive plasma proteins or intrinsically promote cell adhesion (114). Thus, hybrid PEGDA-GAG gels permit the defined investigation of GAG identity on SMC behavior. In addition, the slow degradation rate and high crosslink density of PEGDA gels force encapsulated cells to take on rounded/stellate morphologies with limited cell-cell interactions (115, 116). These particular characteristics of PEGDA hydrogels are generally considered undesirable for the study of normal SMC function. However, they are appropriate for atherosclerotic-mimetic environments, since atherosclerosis-induced changes are associated with SMCs taking on rounded/stellate morphologies (117-119) with limited intercellular gap junctions (120). Finally, the dense crosslinking and slow degradation rate of PEGDA gels prevent cell-mediated hydrogel contraction and the associated changes in scaffold material properties which can confound interpretation of cell responses (115).

In the present work, porcine SMCs were encapsulated in PEGDA hydrogels containing 0.1 wt% GAG, a concentration selected to be consistent with GAG levels in the arterial tissue (109, 121). A 10 wt% 10 kDa PEGDA hydrogel was chosen for the base-scaffold in order to mimic the modulus of lipid-rich regions of grade II atherosclerotic plaque (122). Following 14 and 35 days of culture, SMC phenotype in each formulation was assessed biochemically and histologically.

4.2 Materials and Methods

4.2.1 Polymer Synthesis and Characterization

PEG-Diacrylate Synthesis. PEGDA was prepared as previously described (123) by combining 0.1 mmol/ml dry PEG (10 kDa, Fluka), 0.4 mmol/ml acryloyl chloride, and 0.2 mmol/ml triethylamine in anhydrous dichloromethane (DCM) and stirring under argon overnight. The resulting solution was washed with 2 M K_2CO_3 and separated into aqueous and DCM phases to remove HCl. The DCM phase was subsequently dried with anhydrous $MgSO_4$, and PEGDA was precipitated in diethyl ether, filtered, and dried under vacuum. Extent of PEG diacrylation was determined by ^{1}H-NMR to be ~70%.

Synthesis of Methacrylate-Derivatized CSC and DS. In order to conjugate specific GAGs within the PEGDA-based hydrogel networks, each GAG type was methacrylate-derivatized according to standard protocols (124). CSC (~50 kDa; 6.4 wt% Sulfur; Sigma), and DS (~41.5 kDa; 6.1 wt% Sulfur; Sigma) were selected to have molecular weights (MWs) consistent with those observed in atherosclerotic tissue (108, 121). The respective sulfur contents of these GAG chains indicated that, on average, the

disaccharide units composing the employed CSC and DS had a charge-density associated with mono-sulfation.

The GAGs were dissolved in dIH_2O to achieve a 1 wt% final concentration, and the pH of each solution was adjusted to 8.0. A 10 fold molar excess of methacrylic anhydride (Polysciences) was added per disaccharide unit. Each reaction was allowed to proceed under constant stirring at 4 °C, with the solution pH being maintained at ~8.0 by periodic addition of 5 M NaOH. The product of each reaction was precipitated twice into chilled ethanol 95%, dialyzed against dIH_2O for 48 h, and lyophilized. The extent of methacrylate-derivatization was characterized by ^{1}H-NMR to be ~1.0-1.6%. These levels of methacrylate-derivatization have been previously shown to negligibly alter observed cell responses (115, 124-128).

Synthesis of Methacrylate-Derivatized Intermediate Molecular Weight HA. Recent studies indicate that atherosclerotic vessels contain two primary HA populations, one with MW > $1x10^3$ kDa, which is also present within normal tissue, and a second with MW ~340 kDa, which appears to be specific to atherosclerotic tissue (108, 113). To generate HA appropriate for the examination of atherosclerotic conditions, high MW HA (HA_{HMW}, *Streptococcus equi*, MW ~$1.65x10^3$ kDa; Fluka) was first methacrylate-derivatized as above. The purified product was then dissolved at 1 mg/mL in PBS containing 0.05% sodium azide and 5 U/ml hyaluronidase IV-S (H3884, Sigma). Following incubation at 37 °C overnight, the enzyme was heat-inactivated. The resulting digestion product (HA_{IMW}-MA) was dialyzed against dIH_2O for 48 h and lyophilized.

The mean MW of the isolated HA_{IMW}-MA was determined to be ~400 kDa, with a polydispersity of ~1.3 using gel permeation chromatography (Viscotek).

Synthesis of Acrylate-Derivatized Cell Adhesion Peptide. Cell adhesion peptide RGDS (American Peptide) was reacted with acryloyl-PEG-N-hydroxysuccinimide (ACRL-PEG-NHS, 3.4 kDa, Nektar) at a 1:1 molar ratio for 2 h in 50 mM sodium bicarbonate buffer, pH 8.5 (116). The product (ACRL-PEG-RGDS) was purified by dialysis, lyophilized, and stored at -20 ºC until use.

4.2.2 Characterization of Hydrogel Properties

Hydrogel Initial Water Uptake. To compare initial hydrogel water uptake across formulations, the initial weight (W_i) of each gel was determined immediately following polymerization, after which the gels were submerged in media. After 24 h, the swollen weight (W_s) of each gel was measured. The equilibrium water uptake (S) was calculated as: $S = \left(\frac{W_s}{W_i} \right)$. This information was used to estimate the increase in hydrogel volume due to swelling, data which were then used to compare post-swelling GAG levels across gels.

Average Mesh Size. PEGDA hydrogel mesh size cannot be visualized using standard techniques such as scanning electron microscopy (SEM) (129). In the present study, hydrogel mesh size was characterized via a series of dextran diffusion experiments based on an adaptation of the methodology of Watkins et al.(130) To avoid charge–charge interactions between the diffusing dextrans and the GAG chains in the hydrogel network, fluorescently-labeled, charge-neutral dextrans were employed.

In brief, PEGDA-GAG hydrogels were prepared and allowed to swell overnight at room temperature in PBS containing 0.05% azide (PBS-azide). 8mm diameter discs were cored from each hydrogel formulation. Fluorescently-labeled, charge-neutral dextrans (40 kDa and 70 kDa, Invitrogen) were dissolved at 0.05 mg/mL in PBS-azide and added at 0.5 mL per hydrogel disc (3 discs per dextran MW). Dextran solutions were allowed to diffuse into the hydrogels for 24 h at room temperature. Each gel disc was gently blotted and transferred to 0.5 mL fresh PBS-azide. Dextran that had penetrated into the hydrogels was then permitted to diffuse out into the surrounding solution at room temperature. After 24 h, the fluorescence of the PBS-azide solution surrounding each disc was measured at ex/em 528/590. Dextran standard curves were used to convert each fluorescence signal to a concentration. For each hydrogel formulation, the measured concentration readings for each dextran MW were divided by gel thickness and then plotted versus dextran hydrodynamic radius (131). The area (A) under the resulting curve served as a quantitative indicator of hydrogel permissivity over the hydrodynamic radii range assayed. For the purposes of comparison, the calculated area values for CSC and DS gels were normalized to that of the HA_{IMW} gels to yield a relative mesh size value: $\xi_x \sim \left(\frac{A_x}{A_{HA}}\right)$.

Hydrogel Permissivity to LDL. To confirm the ability of LDL molecules to diffuse into the hydrogel networks, three gels from each formulation were exposed to a 50 μg/mL solution of fluorescently-labeled LDL (Invitrogen) overnight at room temperature. Following 24 h, the levels of LDL which had diffused into the hydrogel

networks were examined using confocal microscopy and compared to control gels which had not been exposed to LDL.

Comparison of GAG LDL Retention. To assess differences in the LDL-binding capacity of the various GAG-laden hydrogels, samples which had been exposed overnight to fluorescently-labeled LDL were transferred to a solution of fresh PBS-azide. Over a period of 24 h, the surrounding PBS solution was exchanged twice, after which the hydrogels were transferred to fresh PBS-solution for fluorescence imaging.

4.2.3 Cell Culture

Cryopreserved aortic SMCs (Cell Applications) isolated from pigs, a common animal model for vascular SMC physiology (132, 133), were thawed and expanded in monolayer culture between passages 4-8. Prior to encapsulation, cells were maintained at 37 ºC/5% CO_2 in Dulbecco's Modified Eagles' Media (DMEM, Hyclone) supplemented with 10% fetal bovine serum (FBS, Hyclone), 1 ng/mL bFGF (BD Biosciences), 100 mU/mL penicillin and 100 mg/L streptomycin (Hyclone).

4.2.4 Cell Encapsulation and Hydrogel Maintenance

Hydrogels were fabricated by preparing precursor solutions containing 100 mg/mL 10 kDa PEGDA, 1 mg/ml of methacrylate-derivatized GAG, and 1 μmol/ml ACRL-PEG-RGDS in HEPES buffered saline (HBS; 10 mM HEPES, 150 mM NaCl, pH 7.4). The concentration of GAG was selected to be consistent with physiological levels in arterial tissue (109). In addition, the 100:1 weight ratio of PEGDA to GAG was chosen to ensure that the degradation rate, modulus, and initial mesh structure of each hydrogel network would be dominated by PEGDA (115). A 300 mg/ml solution of UV

photoinitiator 2,2-dimethoxy-2-phenyl-acetophenone in N-vinylpyrrolidone was added at 1% to each precursor solution. SMCs were harvested and resuspended in the filter-sterilized precursor solutions at ~1x10^6 cells/mL. The cell suspensions were then poured into molds composed of two glass plates separated by 0.5 mm polycarbonate spacers and polymerized by 2 min exposure to longwave UV light (Spectroline, ~6 mW/cm^2, 365 nm). The hydrogel slabs were transferred to Omnitrays (Nunc) fitted with 4 sterile polycarbonate bars to simultaneously prevent gel flotation and prevent gel contact with the tray bottom. Hydrogels were immersed in DMEM supplemented with 10% FBS, 100 mU/mL penicillin, and 100 mg/L streptomycin and maintained at 37 ºC/5 % CO_2. The FBS lot used for the present studies contained ~50 mg/dL LDL according to manufacturer quality control assays.

Hydrogel Mechanical Properties and Contraction. Following initial swelling, three 8 mm diameter samples were cored from each hydrogel. The thickness of each disc was measured using a digital caliper. These thickness measures served both as gauge lengths for mechanical testing as well as indicators of hydrogel degradation and/or SMC-mediated gel compaction with time. Following application of a 0.01 N preload, each hydrogel was subjected to cyclic unconstrained compression (~10% cyclic strain) at 1 Hz using an Instron 3342. The dynamic compressive modulus of each hydrogel formulation was extracted from the resulting stress-strain data.

4.2.5 Endpoint Hydrogel Analyses

At days 14 and 35 of culture, a series of 8 mm diameter samples were collected from each hydrogel formulation for mechanical, biochemical, and histological analyses.

Mechanical samples were tested as described above.

Collagen and Elastin Analyses. Samples harvested for biochemical analyses were transferred to screw-cap vials, weighed, flash-frozen in liquid nitrogen, and stored at -80 ºC until time of analysis. The weight of each 8 mm disc was used as a second indicator of gel degradation and/or compaction, since the reduction in gel volume associated with both of these processes would be reflected in a mass loss, assuming lack of commensurate neomatrix deposition (115). Hydrogel samples were digested for 72 h at 37 ºC in 1 ml of 0.12 M NaOH per 0.2 g hydrogel wet weight (134, 135). DNA, total collagen, and elastin were then analyzed per established protocols. For each assay, the standards used were subjected to the same association with PEGDA and GAG and to the same digestion conditions as the samples. Resulting collagen and elastin data were normalized to cell number.

DNA Analysis. Aliquots of the hydrolyzed samples (n = 12 per formulation) were neutralized and their DNA content determined using the Invitrogen PicoGreen assay (134). DNA measures were translated to cell number using a conversion factor of 6.6 pg DNA per cell (136). Calf thymus DNA (Sigma) served as a standard.

Collagen Analysis. The amino acid hydroxyproline was quantified as an indirect measure of total collagen. In brief, aliquots (n = 4-6 per formulation) collected for collagen quantitation were hydrolyzed for 18 h at 110 °C in 6 M HCl. Each sample was then dried on a Labconco Centrivap to remove HCl, resuspended in dIH_2O, and passed through a charcoal-packed centrifugal microcolumn (Nunc) to remove caramelized sugars. The resultant samples were reacted with chloramine T and p-

dimethylbenzaldehyde reagents (134, 135). Sample absorbance was read at 550 nm relative to that of L-4-hydroxyproline (Sigma). Total collagen content was estimated from measured grams of hydroxyproline by dividing by 0.13 (137).

Elastin Analysis. Elastin production was measured using indirect ELISA (138). NaOH digested samples (n = 9-14 per formulation) were neutralized and further digested with 0.25 M oxalic acid at 100 ºC overnight. Oxalic acid was removed from the samples and exchanged for PBS using Microcon YM-3 centrifugal filters (Millipore). One hundred μL of the resulting samples were applied to a high binding multiwell plate for 3 h at room temperature. After blocking the plate with bovine serum albumin (BSA), adsorbed elastin elastin (Sigma) serving as a standard.

GAG Analyses. Quantification of individual GAG types as well as changes in the levels of specific GAG types requires specialized techniques, which generally rely on the identifying GAG classes based on their characteristic component disaccharides. Given the anticipated levels of neo-GAG synthesis (~ 5 μg/g gel = ~ 50 μg/g PEG) (116), the high sensitivity technique known as fluorescence assisted carbohydrate electrophoresis (FACE) was employed and GAG type assessments were limited to HA, DS, CSC-related disaccharide units.

To isolate newly synthesized GAGs from the GAG chains which had been covalently linked to the PEGDA hydrogel network, a two-step degradation process was employed. This first phase of this process was intended to release newly deposited GAGs and the second step was intended to release GAGs conjugated to the hydrogel network. In brief, harvested hydrogel samples were sliced into a series of 30 μm sections

using a cryomicrotome, after which these sections were exposed to a 1 mg/mL solution of proteinase K (Worthington Biochemical) at 37 °C. Sectioning increased the surface area for enzymatic action, allowing the proteinase K to release GAGs bound to either proteoglycan core proteins or to cell receptors. However, since the covalent bonds linking the methacrylate-derivatized GAGs to the PEGDA chains are not labile by proteinase K, the GAGs conjugated to the hydrogel network were not released by this treatment. Following 24 h of digestion, the samples were heated to inactivate the proteinase K, after which they were centrifuged, and the supernatant collected. The gel sections were then rinsed with PBS, and the wash solution was combined with the initial proteinase K supernatant. The gels sections were then immersed in 0.1 M NaOH for 24 h at 37 °C to induce hydrolysis of the hydrogel structure and the release of conjugated GAG chains as well as of the composing PEG chains.

Each proteinase K supernatant and NaOH treated sample was exposed to 10 mU/µl chondroitinase ABC (*Proteus vulgaris*, Sigma) for 3 h at 37 ºC followed by exposure to 3 µL of 10 mU/µl chondroitinase ACII (*Flavobacterium heparinum*, Seikagaku America) overnight at 37 ºC (139, 140). This enzymatic treatment digested chains of HA, CSC and DS into their component disaccharides, which are primarily ΔDi-HA, ΔDi-6S, and ΔDi-4S, respectively. The chondroitinase ABC/ACII treated samples were then dried, fluorotagged with 2-aminoacridone HCl (Invitrogen) (140), and mixed with glycerol. These samples were then electrophoresed on monosaccharide gels prepared as previously described (140). Negative control samples of pure AMAC were run for each digestion condition. The gel bands were imaged using a Kodak

GelLogic station and analyzed using Image J software. Enzyme digestion products were identified by correspondence to bands in a disaccharide standard lane. The quantity of each disaccharide was determined from the integrated optical density of the band(s), internal maltriose standards, and the aliquot volume used for the enzyme digest (141). The measured disaccharide values were then normalized to total sample PEG content, which was quantified via iodine staining of the electrophoresed hydrolysis samples per Suggs et al (142).

Histological Analyses. Samples harvested for histological analyses were fixed in 10% formalin for 30 min, embedded in Tissue-Tek freezing media, and frozen at -80 ^{o}C. Thirty-five μm sections were cut using a cryomicrotome.

Immunostaining. SMC ECM production and phenotype were analyzed in duplicate sections for each gel sample using standard immunohistochemical technique. All immunostaining steps took place at room temperature unless otherwise noted. Rehydrated sections were blocked with peroxidase for 10 min followed by 10 min exposure to Terminator block (Biocare Medical). Primary antibodies for elastin (BA-4, SCBT), collagen type I (Rockland Immunochemicals), or collagen type III (Rockland Immunochemicals) diluted in PBS-tween (PBS, 0.05% Tween20, 3% BSA) were then applied for 1 h. Primary antibodies for smooth muscle myosin heavy chain (MHC; G-4, SCBT), calponin h1 (CALP, SCBT), A-FABP (C-15, SCBT), and apolipoprotein B (apoB; ab20737, Abcam) were similarly applied to construct sections for 1 h, except that rehydrated sections were permeabilized with PBS-triton (PBS, 0.5% Triton X-100) for 10 min prior to Terminator application. Bound primary antibody was detected by using

AP-conjugated secondary antibody (Jackson Immunochemicals) followed by application of the chromogen Ferangi Blue (Biocare Medical) or by using HRP-conjugated secondary antibody followed by application of the chromogen AEC (LabVision). Based on observed differences in SMC behaviors in CSC and DS gels, day 14 hydrogel samples were also immunostained for metabolic marker glucose 6-phosphate dehydrogenase (G6PD, Abcam) and ECM protein osteocalcin (SCBT) per the above procedure.

Semi-Quantitative Assessments. For intracellular markers (calponin h1, MHC, A-FABP, apoB, and G6PD), cell counts were carried out as semi-quantitative analyses of immunostaining results. These counting assessments were conducted by two independent observers on 2-3 sections (~500-3000 SMC) from each sample according to established methods (143-146). For each cell, i, in a given section, a staining intensity, d_i, was recorded on a scale of 0–3, 0 = "no staining" and 3 = "highest intensity among all treatment groups for that antibody." The cumulative staining intensity, d, for a given antibody in a particular section was calculated using the following equation: $d = (\sum d_i)/(\text{total cell number})$. In addition, since deposited ECM remained localized around the parent cells in each hydrogel formulation, as is characteristic for PEGDA gels (147-149), the relative levels of osteocalcin (day 14 samples only), collagen type I, collagen type III, and elastin, among hydrogel formulations were also evaluated by cell counts per the above procedure. For the purposes of comparison, the resulting cumulative staining intensities for each formulation at a given time point were normalized to the corresponding HA_{IMW} average cumulative staining intensity.

4.2.6 Statistical Analyses

Data were reported as mean ± standard error of the mean. Comparison of sample means was performed by one-way ANOVA and Tukey's post-hoc test (SPSS software), $p < 0.05$.

4.3 Results

4.3.1. Hydrogel Swelling, LDL Permissivity, and Binding Affinity

In order to attribute differences in SMC behavior across hydrogel formulations specifically to initial differences in gel GAG composition, it was important that the remaining hydrogel material properties could be considered consistent across gels. The "bulk" material properties of each gel formulation were therefore characterized and compared. The initial water uptake, S, of each gel following polymerization was similar (CSC: 1.42 ± 0.02, DS: 1.38 ± 0.03, HA_{IMW}: 1.43 ± 0.02), indicating that gel equilibrium hydration could be considered consistent across formulations. The ability of LDL to diffuse through and bind to the GAG-laden hydrogel networks was also characterized by exposing the swollen gels to fluorescently-labeled LDL, examining the equilibrium levels of LDL diffusion, and then assessing LDL retention when the external LDL solution was removed. **Figure 16** demonstrates the ability of LDL to partition into and diffuse evenly throughout the GAG laden hydrogels. When the observed LDL fluorescence intensities within the hydrogel networks were quantified, each hydrogel demonstrated similar permissivity to LDL (**Table 1**). This result was anticipated based on the similarity in bulk average mesh size across hydrogel formulations, as determined

by the equilibrium diffusion of a set of neutral dextrans (**Table 1**), and based on previous reports indicating that the average mesh size of 10% 10kDa PEGDA hydrogels could be considered greater than twice the average hydrodynamic radius of LDL (150)**.** Comparison of LDL retention by the GAG-containing hydrogels following the exchange of the external LDL solution with PBS indicated that each GAG-laden gel had a similar average capacity to bind LDL (**Table 1**).

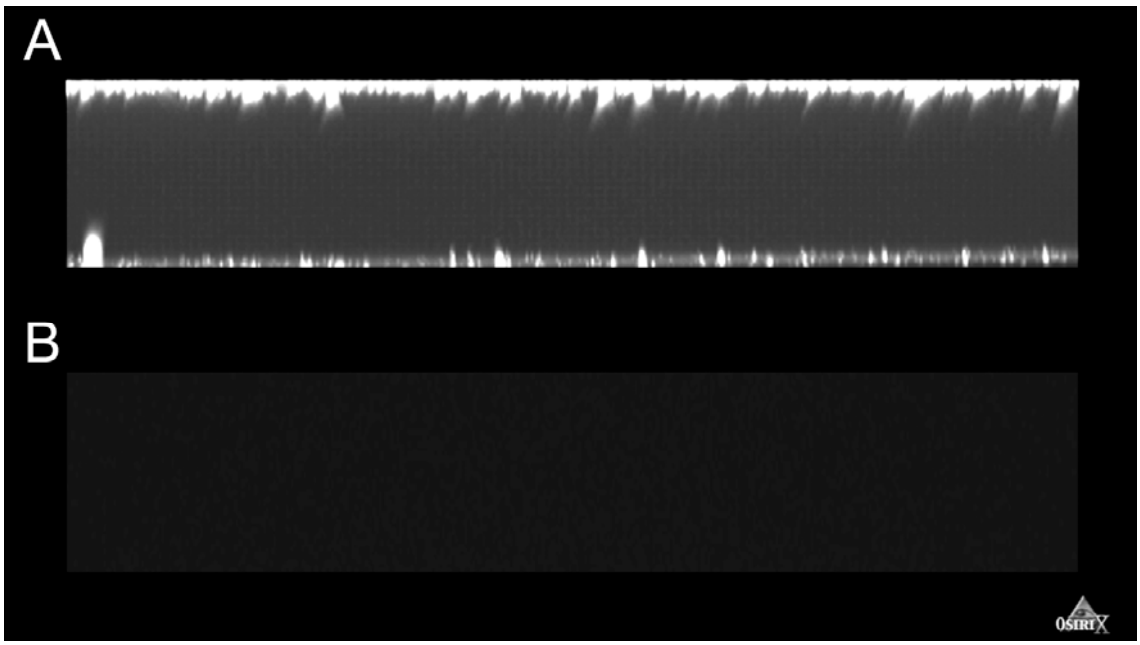

Figure 16. Representative side views of 3D renderings of two, representative confocal image series taken of PEGDA-GAG hydrogels. The upper image is of a hydrogel immersed in a fluorescently labeled LDL solution for 24 h prior to imaging. The external LDL solution is apparent at the upper and lower borders of the gel. The lower image is of a control hydrogel immersed in PBS, rather than LDL, for 24 h prior to imaging. The upper and lower images were generated and rendered using the same microscope and software settings, respectively, to ensure that the grayscale intensities of the hydrogel side-views could be compared.

4.3.2 Assessments of Alterations in GAG Levels and Gel Material Properties

Comparison of initial and endpoint mechanical data (**Table 2**) suggested that average gel modulus could be considered indistinguishable across formulations at each time point. Similarly, the initial and endpoint gel thickness and mass data corresponded to a negligible reduction in gel volume with time (**Table 2**). FACE analysis of the GAGs within hydrolyzed day 0 gels indicated ~100% conjugation of methacrylate-derivatized GAG to the hydrogel networks at the time of polymerization (~11 mg GAG/g PEG = ~ 1.1 mg/mL precursor solution = 0.79 mg/g swollen gel, **Table 3**). Furthermore, the levels of GAGs conjugated to the gel networks at day 14 were not substantially altered from day 0 values. Although the levels of network-conjugated GAGs at day 35 appeared to be decreased relative to time 0 values, these differences were not statistically significant (**Table 3**) due the variation inherent in the FACE and iodine-PEG quantification processes. Cumulatively, the bulk modulus, thickness, gel mass, and conjugated-GAG assessments indicated that the PEGDA-GAG gels retained the slow degradation rate and resistance to cell-mediated contraction characteristic of pure PEGDA hydrogels (134, 148, 151, 152).

Table 1. Hydrogel Relative Mesh Size, LDL Permissivity, and LDL Retention

Gel Type	Relative Mesh Size	LDL Diffusion into Network (μg/g)	LDL Retained (μg/g)
CSC	1.01 ± 0.01	7.52 ± 0.20	0.052 ± 0.028
DS	1.02 ± 0.01	7.37 ± 0.40	0.043 ± 0.013
HA_{IMW}	1.00 ± 0.01	7.52 ± 0.16	0.046 ± 0.019

To assess potential alterations in the GAG types experienced by encapsulated cells due to newly synthesized GAGs, FACE analyses were applied to GAGs released from thin hydrogel sections via exposure to proteinase K. These newly synthesized GAGs were primarily comprised of ΔDi-6S disaccharides (a primary component of CSC; data not shown) in each hydrogel type, and measured between 0.012-0.052 mg/g PEG, which is equivalent to ~0.0008-0.0038 mg GAG/g swollen gel (**Table 3**). In contrast to collagen and elastin, newly synthesized proteoglycans and GAGs are often able to diffuse away from the pericellular space in PEG hydrogels of similar composition to the ones employed herein (116, 148). Therefore, the levels of produced GAGs surrounding cells can be assumed to be significantly lower than the levels of GAGs conjugated to the hydrogel networks.

Table 2. Hydrogel Modulus, Thickness, and Mass Assessments

Gel Type	**Modulus (kPa)**		**Thickness (mm)**		**Mass of 8 mm Discs (mg)**	
	initial	final	initial	final	initial	final
CSC	81.6 ± 3.4	86.6 ± 1.7	0.56 ± 0.01	0.59 ± 0.01	28.4 ± 0.3	29.4 ± 0.3
DS	79.1 ± 2.3	83.0 ± 12.2	0.55 ± 0.01	0.55 ± 0.01	27.6 ± 0.5	27.8 ± 0.4
HA_{IMW}	80.4 ± 3.6	81.5 ± 12.0	0.57 ± 0.01	0.56 ± 0.01	28.7 ± 0.4	28.1 ± 0.5

Table 3. Results from FACE-based GAG Analyses

GAG Source	Gel Type	Initial (mg/g PEG)	Day 14 (mg/g PEG)	Day 35 (mg/g PEG)
Conjugated	**CSC, DS, HA_{IMW}**	11.7 ± 3.0	10.7 ± 3.6	7.0 ± 1.2
Synthesized	**CSC**		0.015 ± 0.003	0.012 ± 0.008
	DS		0.051 ± 0.023	0.018 ± 0.006
	HA_{IMW}		0.052 ± 0.027	0.013 ± 0.006

4.3.3 SMC Collagen and Elastin Deposition

To gauge the extent to which encapsulated SMCs were taking on a synthetic phenotype, elastin and collagen production were analyzed biochemically and histologically at days 14 and 35. As expected for PEGDA gels (147), staining for elastin and individual collagen types was confined to the immediate pericellular space in each formulation (**Figure 17**), enabling reliable semi-quantitative histological analyses of these ECM proteins. Day 14 histological and biochemical data suggested that DS may enhance elastin production relative to HA_{IMW} and CSC (**Figure 18A**). However, for both assessment methods, no statistical differences between elastin levels among hydrogel types were observed. In contrast, day 14 hydroxyproline measures indicated that total collagen levels were significantly higher in DS gels relative to HA_{IMW} gels ($p = 0.014$, **Figure 18B**). Analysis of individual collagen types demonstrated that collagen type I deposition was significantly greater in DS gels than in CSC gels ($p = 0.036$), whereas collagen type III was significantly greater in HA_{IMW} gels relative to both CSC ($p = 0.001$) and DS hydrogels ($p = 0.008$; **Figure 18B**). Comparison of the collagen type I and type

III trends with that of total collagen suggested that collagen type I was the dominant collagen being produced by the encapsulated SMCs. By day 35, differences in elastin production among formulations were no longer apparent (**Figure 18C**), although the day 14 trends in total collagen and collagen type I were maintained at this time-point (**Figure 18D**). In particular, collagen type I deposition at day 35 was greater in DS gels than HA_{IMW} gels ($p = 0.050$). As shown in the notations associated with **Figure 18**, total collagen and total elastin levels per cell remained essentially unaltered from day 14 to day 35, indicating that that the cells had reached a steady-state between the production and degradation of these molecules by day 14.

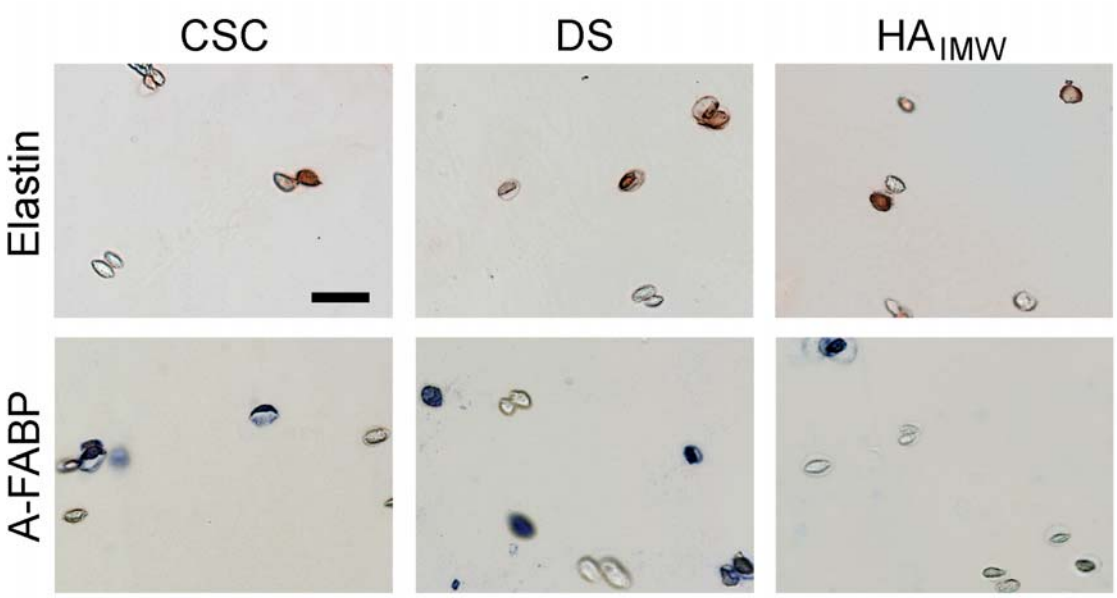

Figure 17. Representative images of day 14 CSC, DS, and HA_{IMW} hydrogel sections immunostained for elastin and A-FABP. The scale bar in the upper-left image represents 40 μm and applies to all images.

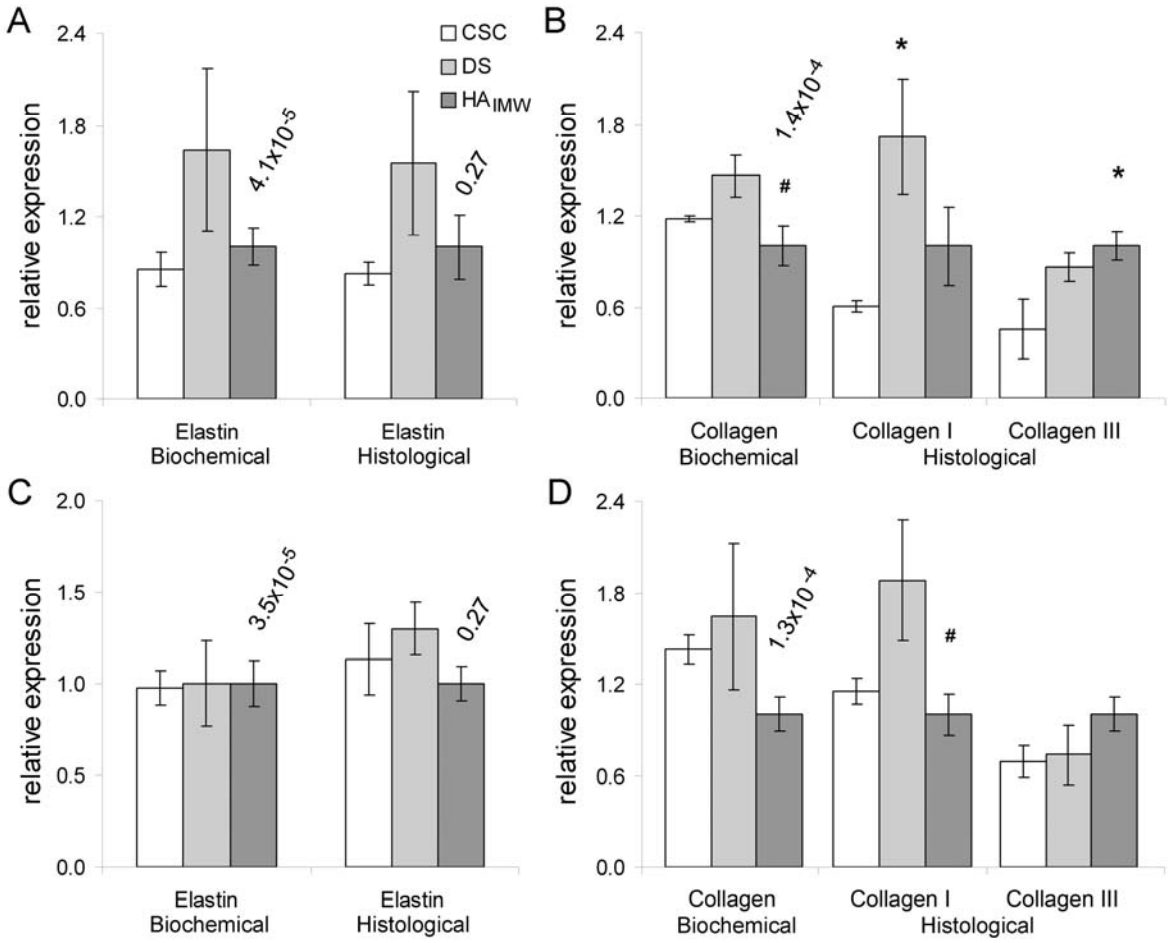

Figure 18. ECM deposition across formulations. (A, C) Relative elastin production by both biochemical and histological assessments at day 14 and day 35, respectively; (B, D) relative total collagen, collagen type I and collagen type III production at day 14 and day 35, respectively. *, significantly different from CSC hydrogels, $p < 0.05$. #, significantly different from DS hydrogels, $p < 0.05$. CSC and DS data at each time point has been normalized to the corresponding HA_{IMW} data, the average values for which are noted above the HA_{IMW} formulation where applicable. For the elastin and collagen biochemical data, the units of the noted values are in micrograms per cell. The noted values for the immunostaining assessments are unitless, but represent both average intensity (on a scale of 1-3) as well as the cell fraction positively stained.

4.3.4 SMC Phenotype

SMC acquisition of adipocyte-like or macrophage-like characteristics was similarly examined (**Figure 19**). At day 14, SMC uptake of LDL (as evidenced by intracellular apoB) was higher in DS gels relative to HA_{IMW} gels ($p = 0.026$; **Figure 19A**). In addition, expression of late-term adipogenic marker A-FABP was significantly greater in CSC ($p = 0.034$) and DS gels ($p = 0.018$) than in HA_{IMW} gels (**Figures 17 and 19A**). By day 35, apoB uptake was greater, not only in DS gels relative to HA_{IMW} gels ($p = 0.028$), but also in CSC gels relative to HA_{IMW} gels ($p = 0.011$). In contrast, only DS gels maintained increased A-FABP expression relative to HA_{LMW} gels at day 35 ($p < 0.001$; **Figure 19C**).

The degree to which encapsulated cells displayed markers associated with a mature, contractile SMC phenotype was also investigated through analysis of calponin h1 and MHC expression. At day 14, calponin h1 levels were greater in DS gels relative to both CSC ($p = 0.021$) and HA_{IMW} ($p = 0.011$) constructs (**Figures 19B**). In contrast, MHC measures indicated that both DS ($p = 0.011$) and HA_{IMW} ($p = 0.039$) supported more contractile phenotypes than CSC. By day 35, calponin h1 expression had leveled out among formulations, and MHC trends had shifted, with HA_{IMW} gels supporting greater MHC expression than either DS ($p = 0.050$) or CSC ($p = 0.048$) gels (**Figure 19D**).

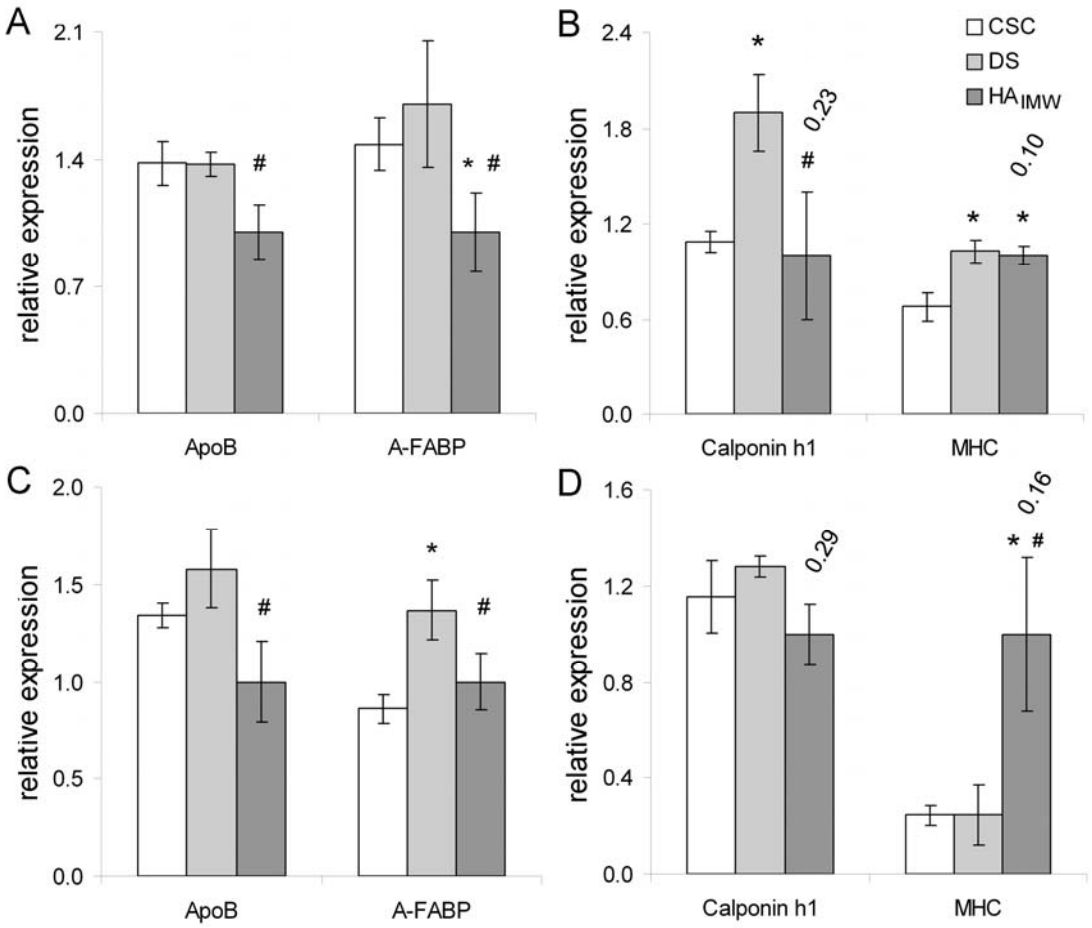

Figure 19. Evaluation of SMC foam cell versus contractile phenotypes. (A, C) Relative apoB uptake and A-FABP expression at day 14 and day 35, respectively. (B, D) Relative expression of markers of a SMC contractile apparatus at day 14 and day 35, respectively. *, significantly different from CSC hydrogels, $p < 0.05$. #, significantly different from DS hydrogels, $p < 0.05$. CSC and DS data at each time point has been normalized to the corresponding HA_{IMW} data, the average values for which are noted above the HA_{IMW} formulation where applicable. The noted values for the immunostaining assessments are unitless but represent both average intensity (on a scale of 1-3) as well as the cell fraction positively stained.

Due to the observed differences between the apoB and A-FABP profiles of CSC and DS gels, day 14 hydrogel samples were also immunostained for G6PD and osteocalcin in order to gain further insight into the cell responses within these gels. G6PD is a key metabolic enzyme associated with a primarily anabolic pathway essential in the regulation of oxidative stress (153, 154), one of the stressors in atherosclerosis. In addition, osteocalcin is an ECM protein produced by foam cells in calcific plaques. As shown in **Figure 20,** both G6PD and osteocalcin were elevated in DS gels relative to remaining hydrogel formulations ($p < 0.05$).

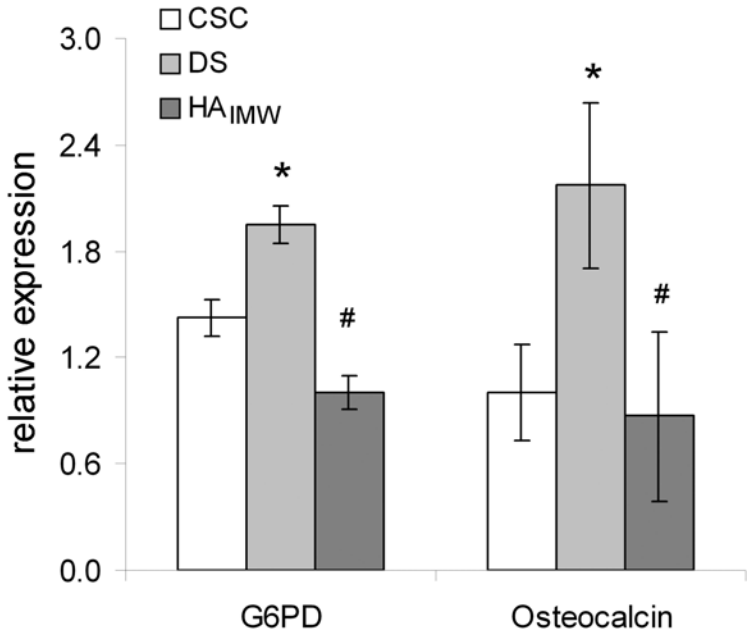

Figure 20. Relative G6PD and osteocalcin expression at day 14. *, significantly different from CSC hydrogels, $p < 0.05$. #, significantly different from DS hydrogels, $p < 0.05$.

4.4 Discussion

The aim of the present study was to examine the impact of GAG type on SMC acquisition of adipocyte-like or macrophage-like characteristics within an environment mimetic of early atherosclerosis. The results from the aforementioned apoB and A-FABP analyses suggest that SMCs in both CSC and DS gels were driven to take on more a macrophage-like phenotype than SMCs in HA_{IMW} gels. However, only cells in DS gels displayed a higher expression of adipocyte marker A-FABP relative to cells in HA_{IMW} gels at both days 14 and 35. Combined, these results indicate that both CSC and DS support greater foam cell formation than HA_{IMW}. However, the mechanisms by which they induce this phenotype transition may be distinct, a possibility supported by the day 14 G6PD and osteocalcin data.

To assess the extent to which SMC acquisition of foam cell characteristics was correlated with a transition toward a synthetic phenotype, SMC collagen and elastin production was evaluated. No consistent differences in SMC elastin deposition were observed over the course of the present study. This result is in agreement with the literature, which indicates that, although changes in elastin levels are at times observed in atherosclerotic lesions, these alterations are generally not consistent in their directionality (155). Instead, changes in elastic fiber structure characterize atherosclerotic vessels (155). Regarding collagen, DS gels displayed greater deposition of collagen type I than CSC and HA_{IMW} gels at both day 14 and day 35. The literature indicates that SMC synthesis of total collagen in general, and of collagen type I in particular, is upregulated in early atherosclerotic lesions (104, 156, 157). Cumulatively,

the present ECM data suggest that DS induces a more synthetic SMC phenotype than CSC or HA_{IMW}, in agreement with the increased foam cell transition observed for DS relative to HA_{IMW}.

The increase in SMC acquisition of a synthetic phenotype in DS gels and of a foam cell phenotype in both CSC and DS gels was not, at least initially, marked by a corresponding decrease in SMC contractile marker expression. Although day 14 data indicated decreased MHC expression in CSC gels relative to HA_{IMW} gels, no decrease was observed in SMC calponin h1 expression between CSC and HA_{IMW} gels at this time-point. Furthermore, day 14 calponin h1 levels were greater in DS gels relative HA_{IMW} gels. Only day 35 MHC measures suggested that the increased foam cell phenotype associated with SMCs in DS gels was being mirrored in the decreased expression of a contractile phenotype. An increase in SMC contractile marker expression in early atherogenesis followed by a down-regulation of these markers in later atherosclerotic stages has previously been documented. For instance, a recent study of SMCs in the aortic arch of LDL-receptor knockout mice revealed increased MHC expression in high cholesterol mice by day 28, coincident with the SMC proliferation and ECM remodeling associated with early atherosclerosis (158). However, by day 98, SMC MHC expression in the advancing atherosclerotic lesions had decreased (158). Combined, the present foam cell, synthetic, and contractile phenotype characterization results indicate that CSC and DS may be involved in the SMC phenotypic modulation associated with atherosclerosis (159).

The apparent link between CSC and DS and SMC foam cell formation suggested by the present results is in agreement with current literature. Specifically, both versican (a proteoglycan which bears primarily CSC and CSA side chains), and biglycan (CS/DS-containing small leucine-rich proteoglycan) have been the focus of several recent studies of proteoglycan involvement in early atherosclerotic lipid deposition (10, 99, 103, 160-162). However, the above comparisons with in vivo data must be interpreted with caution due to the simplified in vitro system used herein.

Several limitations of the present manuscript merit comment. Although we mimicked the cell morphology and limited intercellular junctions associated with SMCs within atherosclerotic lesions, we did not reproduce several other aspects of early atherogenesis. Specifically, the proliferation and migration associated with SMC response to arterial wall injury were not mirrored. Indeed, SMC proliferation and migration were essentially prevented by same PEGDA hydrogel properties which permitted us to induce rounded/stellate SMC phenotypes. Furthermore, the origins of SMC rounding in atherosclerotic environments, which are linked to changes in ECM composition as well as SMC integrin profiles, were not recapitulated (118). The present work also did not fully replicate the complex cascade of events/interactions between several cell types, growth factors, cytokines, and ECM molecules which ultimately lead to the formation of atheromatous plaques (102, 163). Similarly, the role of the PG core protein in modulating SMC response to CSC or DS signals was not accounted for.

Finally, as previously discussed, the interaction of LDL with GAG chains is ionic in nature (161). Thus, GAG chain length and charge densities are determining factors in

the levels of lipid binding per chain (161, 162). Although we have attempted to mimic the GAG chain lengths associated with atherosclerotic vessels in the present work, the CSC and DS chains conjugated to the hydrogel networks may not have charge densities appropriate to the atherogenic environment (164). That being said, we have reported the sulfur levels within the DS and CSC chains employed herein, which should allow appropriate comparison with future work.

Combined, the present results supported the hypothesis that specific GAG types have differential influence on SMC foam cell formation. Specifically, both CSC and DS were associated with greater phagocytosis of apoB relative to HA_{IMW}, although only DS led to sustained increases in A-FABP expression. In DS gels, increased SMC acquisition of foam cell phenotypes was correlated with an increased synthetic phenotype as well as in initial increase in the expression of contractile marker calponin h1. However, over the longer term, SMC expression of contractile markers in both CSC and DS gels decreased relative to that in HA_{IMW} gels. The present model system can be expanded to probe the impact of a range of atherogenic stimuli on SMC phenotype, potentially leading to more effective treatments for atherosclerosis.

CHAPTER V

CONCLUSIONS AND FUTURE WORK

In this project, we first demonstrated that a multi-component scaffold comprised of polyurethane electrospun mesh layers (intended to be mimetic of arterial collagen fiber loading) bonded together by a fibrin hydrogel matrix (intended to be mimetic of arterial elastic fiber response) results in a composite construct which retains the high tensile strength and suture retention strength of electrospun mesh but which displays a "J-shaped" mechanical response similar to that of native coronary artery. To better our design in the future, material properties tuning of the polyurethane-based elastomers can be exploited to identify formulation that show desired mechanical properties and optimal degradation rates. Furthermore, optimization of the fibrin gel composition and composite construct fabrication protocol will also be focused on to improve the layer-layer cohesion.

In order to create functional tissue engineered vascular grafts, well organized mature SMCs are required. The study of cell-material interactions can give the insight on designing appropriate biomaterials to regulate smooth muscle phenotype. In order to remove the biochemical signal from fibrin, we decided to choose inert hydrogel system, such as PEGDA. By using PEGDA hydrogel system, we incorporated ECM proteins, such as fibronectin, fibrinogen, laminin, and collagen type IV into the scaffolds in a more controlled manner. After 7 days of culture without additional growth factors, the relative expression of differentiation markers, activation of cell signaling switches, and

the adhesion receptor integrin profile of smooth muscle precursor 10T½ cells were carefully examined. Surprisingly to us, no significant difference was detected in all the three aspects. It suggests that ECM protein identity is a weak variable in driving progenitor cell differentiation at least at the concentration studied.

To further study the cell-material interactions, we chose another family of ECM componets, glycosaminoglycans (GAGs). Cumulatively, the present results supported the hypothesis that specific GAG types have differential influence on SMC foam cell formation. Both CSC and DS showed higher apoB uptake relative to HA_{IMW}, although only DS had sustained elevation in A-FABP expression. The increased SMC acquisition of a foam cell phenotype in DS gels was associated with an increased synthetic phenotype and a decreased expression of contractile marker MHC as well at day 35. Increases in the amount of externally applied LDL, which was maintained at relatively low levels in the current work, would be expected to enhance observed differences among hydrogel formulations.

From all the previous literature, a lot of ECM properties other than the ECM identity can also be important in determining the cell fates of progenitor cells, such as ECM geometry/topography (57), ECM stiffness (54), control of cell morphology (165) and etc. For instance, impact of cell orientation on cellular behavior can be studied using transparency-based photolithographic patterning method described previously (166, 167). The RGDS patterns and cell patterns are shown in **Figure 21**, four different masks, namely, stripes, checkers, loops, half loops, were used here to assess the impact of

different cell orientations. As shown in **Figure 21**, cells in stripe pattern showed much better alignment than checkers and others.

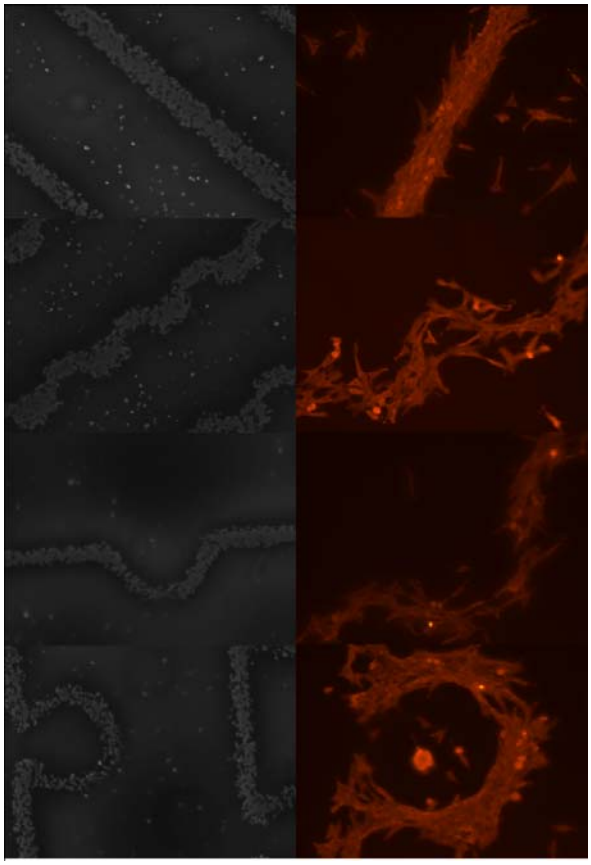

Figure 21. RGDS patterning on PEGDA hydrogel (left panel) and cell patterning on top of the RGDS patterning (right panel).

In order to improve our design of biomaterials and tissue engineered grafts, a better understanding of cell material interactions would never be overemphasized. In the future, study of cell material interactions from other aspects, mainly on cell orientation and cell morphology would be performed to give more insight into tissue engineering applications.

REFERENCES

1. Ratcliffe, A. Tissue engineering of vascular grafts. Matrix Biol. 19(4): 353-357. 2000.

2. Tu, J.V., Pashos, C.L., Naylor, C.D., Chen, E.L., Normand, S.L., Newhouse, J.P., McNeil, B.J. Use of cardiac procedures and outcomes in elderly patients with myocardial infarction in the United States and Canada. New England Journal of Medicine. 336(21): 1500-1505. 1997.

3. Lloyd-Jones. Heart disease and stroke statistics-2009 update: a report from the American Heart Association Statistics Committee and Stroke Statistics Subcommittee. Circulation. 119(3): 480-486. 2009.

4. McKee, J.A., Banik, S.S., Boyer, M.J., Hamad, N.M., Lawson, J.H., Niklason, L.E., Counter, C.M. Human arteries engineered in vitro. EMBO Reports. 4(6): 633-638. 2003.

5. Nerem, R.M., Seliktar, D. Vascular tissue engineering. Annual Review of Biomedical Engineering. 3: 225-243. 2001.

6. Hahn, M.S., McHale, M.K., Wang, E., Schmedlen, R.H., West, J.L. Physiologic pulsatile flow bioreactor conditioning of poly(ethylene glycol)-based tissue engineered vascular grafts. Annals of Biomedical Engineering. 35(2): 190-200. 2007.

7. Lafleur, M.A., Handsley, M.M., Edwards, D.R. Metalloproteinases and their inhibitors in angiogenesis. Expert Reviews in Molecular Medicine. 5(23): 1-39. 2003.

8. Langer, R., Vacanti, J.P. Tissue engineering. Science. 260(5110): 920-926. 1993.

9. Griffith, L.G., Naughton, G. Tissue engineering - current challenges and expanding opportunities. Science. 295(5557): 1009-1014. 2002.

10. Nakashima, Y., Wight, T.N., Sueishi, K. Early atherosclerosis in humans: role of diffuse intimal thickening and extracellular matrix proteoglycans. Cardiovasc. Res. 79(1): 14-23. 2008.

11. John, L.C. Biomechanics of coronary artery and bypass graft disease: potential new approaches. The Annals of Thoracic Surgery. 87(1): 331-338. 2009.

12. van Andel, C.J., Pistecky, P.V., Borst, C. Mechanical properties of porcine and human arteries: implications for coronary anastomotic connectors. The Annals of Thoracic Surgery. 76(1): 58-64. 2003.

13. Roach, M.R., Burton, A.C. The reason for the shape of the distensibility curves of arteries. Canadian Journal of Biochemistry and Physiology. 35(8): 681-690. 1957.

14. Seliktar, D., Black, R.A., Vito, R.P., Nerem, R.M. Dynamic mechanical conditioning of collagen-gel blood vessel constructs induces remodeling in vitro. Annals of Biomedical Engineering. 28(4): 351-362. 2000.

15. Isenberg, B.C., Tranquillo, R.T. Long-term cyclic distention enhances the mechanical properties of collagen-based media-equivalents. Annals of Biomedical Engineering. 31(8): 937-949. 2003.

16. Solan, A., Mitchell, S., Moses, M., Niklason, L. Effect of pulse rate on collagen deposition in the tissue-engineered blood vessel. Tissue Engineering. 9(4): 579-586. 2003.

17. Ma, Z.W., Kotaki, M., Inai, R., Ramakrishna, S. Potential of nanofiber matrix as tissue-engineering scaffolds. Tissue Engineering. 11(1-2): 101-109. 2005.

18. Bashur, C.A., Dahlgren, L.A., Goldstein, A.S. Effect of fiber diameter and orientation on fibroblast morphology and proliferation on electrospun poly(D,L-lactic-co-glycolic acid) meshes. Biomaterials. 27(33): 5681-5688. 2006.

19. Guelcher, S.A. Biodegradable polyurethanes: synthesis and applications in regenerative medicine. Tissue Engineering Part B Review. 14(1): 3-17. 2008.

20. Guelcher, S.A., Srinivasan, A., Dumas, J.E., Didier, J.E., McBride, S., Hollinger, J.O. Synthesis, mechanical properties, biocompatibility, and biodegradation of polyurethane networks from lysine polyisocyanates. Biomaterials. 29(12): 1762-1775. 2008.

21. Guelcher, S.A., Gallagher, K.M., Didier, J.E., Klinedinst, D.B., Doctor, J.S., Goldstein, A.S., Wilkes, G.L., Beckman, E.J., Hollinger, J.O. Synthesis of biocompatible segmented polyurethanes from aliphatic diisocyanates and diurea diol chain extenders. Acta biomaterialia. 1(4): 471-484. 2005.

22. Kavlock, K.D., Pechar, T.W., Hollinger, J.O., Guelcher, S.A., Goldstein, A.S. Synthesis and characterization of segmented poly(esterurethane urea) elastomers for bone tissue engineering. Acta Biomaterialia. 3(4): 475-484. 2007.

23. Soletti, L., Hong, Y., Guan, J., Stankus, J.J., El-Kurdi, M.S., Wagner, W.R., Vorp, D.A. A bilayered elastomeric scaffold for tissue engineering of small diameter vascular grafts. Acta Biomaterialia. 6(1): 110-122. 2010.

24. Stylianopoulos, T., Bashur, C.A., Goldstein, A.S., Guelcher, S.A., Barocas, V.H. Computational predictions of the tensile properties of electrospun fibre meshes: effect of fibre diameter and fibre orientation. Journal of the Mechanical Behavior of Biomedical Materials. 1(4): 326-335. 2008.

25. Drury, J.L., Mooney, D.J. Hydrogels for tissue engineering: scaffold design variables and applications. Biomaterials. 24(24): 4337-4351. 2003.

26. Spotnitz, W.D. Fibrin sealant: past, present, and future: a brief review. World Journal of Surgery. 34(4): 632-634. 2010.

27. Ahmann, K.A., Weinbaum, J.S., Johnson, S.L., Tranquillo, R.T. Fibrin degradation enhances vascular smooth muscle cell proliferation and matrix deposition in fibrin-based tissue constructs fabricated in vitro. Tissue Engineering Part A. 16(10): 3261-3270. 2010.

28. Huynh, T.N., Tranquillo, R.T. Fusion of concentrically layered tubular tissue constructs increases burst strength. Annals of Biomedical Engineering. 38(6): 2226-2236. 2010.

29. Long, J.L., Tranquillo, R.T. Elastic fiber production in cardiovascular tissue-equivalents. Matrix Biol. 22(4): 339-350. 2003.

30. Tranquillo, R.T., Girton, T.S., Bromberek, B.A., Triebes, T.G., Mooradian, D.L. Magnetically orientated tissue-equivalent tubes: application to a circumferentially orientated media-equivalent. Biomaterials. 17(3): 349-357. 1996.

31. Liu, H., Collins, S.F., Suggs, L.J. Three-dimensional culture for expansion and differentiation of mouse embryonic stem cells. Biomaterials. 27(36): 6004-6014. 2006.

32. Zhang, G., Wang, X.H., Wang, Z.L., Zhang, J.Y., Suggs, L. A PEGylated fibrin patch for mesenchymal stem cell delivery. Tissue Engineering. 12(1): 9-19. 2006.

33. Munoz-Pinto, D.J., Jimenez-Vergara, A.C., Gelves, L.M., McMahon, R.E., Guiza-Arguello, V., Hahn, M.S. Probing vocal fold fibroblast response to

hyaluronan in 3D contexts. Biotechnology and Bioengineering. 104(4): 821-831. 2009.

34. Bashur, C.A., Shaffer, R.D., Dahlgren, L.A., Guelcher, S.A., Goldstein, A.S. Effect of fiber diameter and alignment of electrospun polyurethane meshes on mesenchymal progenitor cells. Tissue Engineering. 15(9): 2435-2445. 2009.

35. Johnson, C.P., How, T., Scraggs, M., West, C.R., Burns, J. A biomechanical study of the human vertebral artery with implications for fatal arterial injury. Forensic Science International 109(3): 169-182. 2000.

36. Bulick, A.S., Munoz-Pinto, D.J., Qu, X., Mani, M., Cristancho, D., Urban, M., Hahn, M.S. Impact of endothelial cells and mechanical conditioning on smooth muscle cell extracellular matrix production and differentiation. Tissue Engineering Part A. 15(4): 815-825. 2009.

37. Hirschi, K.K., Lai, L., Belaguli, N.S., Dean, D.A., Schwartz, R.J., Zimmer, W.E. Transforming growth factor-beta induction of smooth muscle cell phenotype requires transcriptional and post-transcriptional control of serum response factor. The Journal of Biological Chemistry. 277(8): 6287-6295. 2002.

38. Hirschi, K.K., Rohovsky, S.A., D'Amore, P.A. PDGF, TGF-beta, and heterotypic cell-cell interactions mediate endothelial cell-induced recruitment of 10T1/2 cells and their differentiation to a smooth muscle fate. The Journal of Cell Biology. 141(3): 805-814. 1998.

39. Syedain, Z.H., Weinberg, J.S., Tranquillo, R.T. Cyclic distension of fibrin-based tissue constructs: evidence of adaptation during growth of engineered connective tissue. Proc. Natl. Acad. Sci. U. S. A. 105(18): 6537-6542. 2008.

40. Posey, J., Geddes, L. Measurement of the modulus of elasticity of the arterial wall. Cardiovasc. Res. Ctr. Bull. 111(4): 83-103. 1973.

41. Bryant, S.J., Nuttelman, C.R., Anseth, K.S. Cytocompatibility of UV and visible light photoinitiating systems on cultured NIH/3T3 fibroblasts in vitro. Journal of Biomaterials Science. 11(5): 439-457. 2000.

42. Lu, X., Pandit, A., Kassab, G.S. Biaxial incremental homeostatic elastic moduli of coronary artery: two-layer model. American Journal of Physiology. 287(4): H1663-1669. 2004.

43. Weinberg, C.B., Bell, E. A blood vessel model constructed from collagen and cultured vascular cells. Science. 231(4736): 397-400. 1986.

44. Chesler, N.C., Ku, D.N., Galis, Z.S. Transmural pressure induces matrix-degrading activity in porcine arteries ex vivo. The American Journal of Physiology. 277(5): H2002-2009. 1999.

45. Hasaneen, N.A., Zucker, S., Cao, J., Chiarelli, C., Panettieri, R.A., Foda, H.D. Cyclic mechanical strain-induced proliferation and migration of human airway smooth muscle cells: role of EMMPRIN and MMPs. FASEB J. 19(11): 1507-1509. 2005.

46. Mills, I., Cohen, C.R., Kamal, K., Li, G., Shin, T., Du, W., Sumpio, B.E. Strain activation of bovine aortic smooth muscle cell proliferation and alignment: study of strain dependency and the role of protein kinase A and C signaling pathways. Journal of Cellular Physiology. 170(3): 228-234. 1997.

47. Ekaputra, A.K., Prestwich, G.D., Cool, S.M., Hutmacher, D.W. Combining electrospun scaffolds with electrosprayed hydrogels leads to three-dimensional cellularization of hybrid constructs. Biomacromolecules. 9(8): 2097-2103. 2008.

48. Nieponice, A., Soletti, L., Guan, J., Deasy, B.M., Huard, J., Wagner, W.R., Vorp, D.A. Development of a tissue-engineered vascular graft combining a biodegradable scaffold, muscle-derived stem cells and a rotational vacuum seeding technique. Biomaterials. 29(7): 825-833. 2008.

49. Bhatia, R., Hare, J.M. Mesenchymal stem cells: future source for reparative medicine. Congestive Heart Failure. 11(2): 87-91. 2005.

50. Au, P., Tam, J., Fukumura, D., Jain, R.K. Bone marrow-derived mesenchymal stem cells facilitate engineering of long-lasting functional vasculature. Blood. 111(9): 4551-4558. 2008.

51. Narita, Y., Yamawaki, A., Kagami, H., Ueda, M., Ueda, Y. Effects of transforming growth factor-beta 1 and ascorbic acid on differentiation of human bone-marrow-derived mesenchymal stem cells into smooth muscle cell lineage. Cell Tissue Res. 333(3): 449-459. 2008.

52. Kim, P.D., Peyton, S.R., VanStrien, A.J., Putnam, A.J. The influence of ascorbic acid, TGF-beta1, and cell-mediated remodeling on the bulk mechanical properties of 3-D PEG-fibrinogen constructs. Biomaterials. 30(23-24): 3854-3864. 2009.

53. Treguer, K., Naye, F., Thiebaud, P., Fedou, S., Soulet, F., Theze, N., Faucheux, C. Smooth muscle cell differentiation from human bone marrow: variations in

cell type specific markers and Id gene expression in a new model of cell culture. Cell Biol. Int. 33(6): 621-631. 2009.

54. Engler, A.J., Sen, S., Sweeney, H.L., Discher, D.E. Matrix elasticity directs stem cell lineage specification. Cell. 126(4): 677-689. 2006.

55. Salasznyk, R.M., Williams, W.A., Boskey, A., Batorsky, A., Plopper, G.E. Adhesion to vitronectin and collagen I promotes osteogenic differentiation of human mesenchymal stem cells. J. Biomed. Biotechnol. 2004(1): 24-34. 2004.

56. Klees, R.F., Salasznyk, R.M., Kingsley, K., Williams, W.A., Boskey, A., Plopper, G.E. Laminin-5 induces osteogenic gene expression in human mesenchymal stem cells through an ERK-dependent pathway. Mol. Biol. Cell. 16(2): 881-890. 2005.

57. Guilak, F., Cohen, D.M., Estes, B.T., Gimble, J.M., Liedtke, W., Chen, C.S. Control of stem cell fate by physical interactions with the extracellular matrix. Cell Stem Cell. 5(1): 17-26. 2009.

58. Hungerford, J.E., Little, C.D. Developmental biology of the vascular smooth muscle cell: building a multilayered vessel wall. Journal of Vascular Research. 36(1): 2-27. 1999.

59. Carmeliet, P. Angiogenesis in health and disease. Nature Medicine. 9(6): 653-660. 2003.

60. Risau, W., Lemmon, V. Changes in the vascular extracellular matrix during embryonic vasculogenesis and angiogenesis. Dev. Biol. 125(2): 441-450. 1988.

61. George, E.L., Georges-Labouesse, E.N., Patel-King, R.S., Rayburn, H., Hynes, R.O. Defects in mesoderm, neural tube and vascular development in mouse embryos lacking fibronectin. Development. 119(4): 1079-1091. 1993.

62. Drake, C.J., Davis, L.A., Walters, L., Little, C.D. Avian vasculogenesis and the distribution of collagens I, IV, laminin, and fibronectin in the heart primordia. The Journal of Experimental Zoology. 255(3): 309-322. 1990.

63. Ruger, B.M., Breuss, J., Hollemann, D., Yanagida, G., Fischer, M.B., Mosberger, I., Chott, A., Lang, I., Davis, P.F., Hocker, P., Dettke, M. Vascular morphogenesis by adult bone marrow progenitor cells in three-dimensional fibrin matrices. Differentiation. 76(7): 772-783. 2008.

64. Lien, S.C., Usami, S., Chien, S., Chiu, J.J. Phosphatidylinositol 3-kinase/Akt pathway is involved in transforming growth factor-beta1-induced phenotypic

modulation of 10T1/2 cells to smooth muscle cells. Cellular signalling. 18(8): 1270-1278. 2006.

65. Miller, S.A., Brown, A.J., Farach-Carson, M.C., Kirn-Safran, C.B. HIP/RPL29 down-regulation accompanies terminal chondrocyte differentiation. Differentiation. 71(6): 322-336. 2003.

66. Sato, M., Kawai-Kowase, K., Sato, H., Oyama, Y., Kanai, H., Ohyama, Y., Suga, T., Maeno, T., Aoki, Y., Tamura, J., Sakamoto, H., Nagai, R., Kurabayashi, M. c-Src and hydrogen peroxide mediate transforming growth factor-beta1-induced smooth muscle cell-gene expression in 10T1/2 cells. Arteriosclerosis, Thrombosis, and Vascular Biology. 25(2): 341-347. 2005.

67. Wang, J., Li, A., Wang, Z., Feng, X., Olson, E.N., Schwartz, R.J. Myocardin sumoylation transactivates cardiogenic genes in pluripotent 10T1/2 fibroblasts. Molecular and Cellular Biology. 27(2): 622-632. 2007.

68. Pampaloni, F., Reynaud, E.G., Stelzer, E.H. The third dimension bridges the gap between cell culture and live tissue. Nature Reviews Molecular Cell Biology. 8(10): 839-845. 2007.

69. Nguyen, K.T., West, J.L. Photopolymerizable hydrogels for tissue engineering applications. Biomaterials. 23(22): 4307-4314. 2002.

70. Greenwald, R.B., Conover, C.D., Choe, Y.H. Poly(ethylene glycol) conjugated drugs and prodrugs: a comprehensive review. Critical Reviews in Therapeutic Drug Carrier Systems. 17(2): 101-161. 2000.

71. Rizzi, S.C., Ehrbar, M., Halstenberg, S., Raeber, G.P., Schmoekel, H.G., Hagenmuller, H., Muller, R., Weber, F.E., Hubbell, J.A. Recombinant protein-co-PEG networks as cell-adhesive and proteolytically degradable hydrogel matrixes. Part II: biofunctional characteristics. Biomacromolecules. 7(11): 3019-3029. 2006.

72. Lee, W.K., Ichi, T., Ooya, T., Yamamoto, T., Katoh, M., Yui, N. Novel poly(ethylene glycol) scaffolds crosslinked by hydrolyzable polyrotaxane for cartilage tissue engineering. Journal of Biomedical Materials Research. 67(4): 1087-1092. 2003.

73. Halstenberg, S., Panitch, A., Rizzi, S., Hall, H., Hubbell, J.A. Biologically engineered protein-graft-poly(ethylene glycol) hydrogels: a cell adhesive and plasmin-degradable biosynthetic material for tissue repair. Biomacromolecules. 3(4): 710-723. 2002.

74. Lee, H.J., Lee, J.S., Chansakul, T., Yu, C., Elisseeff, J.H., Yu, S.M. Collagen mimetic peptide-conjugated photopolymerizable PEG hydrogel. Biomaterials. 27(30): 5268-5276. 2006.

75. Hahn, M.S., Taite, L.J., Moon, J.J., Rowland, M.C., Ruffino, K.A., West, J.L. Photolithographic patterning of polyethylene glycol hydrogels. Biomaterials. 27(12): 2519-2524. 2006.

76. Roberts, M.J., Bentley, M.D., Harris, J.M. Chemistry for peptide and protein PEGylation. Advanced Drug Delivery Reviews. 54(4): 459-476. 2002.

77. Hern, D.L., Hubbell, J.A. Incorporation of adhesion peptides into nonadhesive hydrogels useful for tissue resurfacing. Journal of Biomedical Materials Research. 39(2): 266-276. 1998.

78. Hummon, A.B., Lim, S.R., Difilippantonio, M.J., Ried, T. Isolation and solubilization of proteins after TRIzol extraction of RNA and DNA from patient material following prolonged storage. Biotechniques. 42(4): 467-470. 2007.

79. Wang, E.A., Israel, D.I., Kelly, S., Luxenberg, D.P. Bone morphogenetic protein-2 causes commitment and differentiation in C3H10T1/2 and 3T3 cells. Growth Factors. 9(1): 57-71. 1993.

80. Chien, C.M., Cheng, J.L., Chang, W.T., Tien, M.H., Wu, W.Y., Chang, Y.H., Chang, H.Y., Chen, S.T. Cell phenotype high analysis using a cell fluid-based microchip with sensitivity and accurate quantitation. Journal of Chromatography B-Analytical Technologies in the Biomedical and Life Sciences. 795(1): 1-8. 2003.

81. Wang, M., Su, Y., Sun, H., Wang, T., Yan, G., Ran, X., Wang, F., Cheng, T., Zou, Z. Induced endothelial differentiation of cells from a murine embryonic mesenchymal cell line C3H/10T1/2 by angiogenic factors in vitro. Differentiation. 79(1): 21-30. 2010.

82. Chamberlain, G., Wright, K., Rot, A., Ashton, B., Middleton, J. Murine mesenchymal stem cells exhibit a restricted repertoire of functional chemokine receptors: comparison with human. PloS One. 3(8): e2934. 2008.

83. Ruoslahti, E. Integrins. The Journal of Clinical Investigation. 87(1): 1-5. 1991.

84. Giancotti, F.G., Ruoslahti, E. Integrin signaling. Science. 285(5430): 1028-1032. 1999.

85. Sobue, K., Hayashi, K., Nishida, W. Expressional regulation of smooth muscle cell-specific genes in association with phenotypic modulation. Molecular and Cellular Biochemistry. 190(1-2): 105-118. 1999.

86. Chang, L., Karin, M. Mammalian MAP kinase signalling cascades. Nature. 410(6824): 37-40. 2001.

87. Chen, Q., Kinch, M.S., Lin, T.H., Burridge, K., Juliano, R.L. Integrin-mediated cell adhesion activates mitogen-activated protein kinases. The Journal of Biological Chemistry. 269(43): 26602-26605. 1994.

88. Zhu, X., Assoian, R.K. Integrin-dependent activation of MAP kinase: a link to shape-dependent cell proliferation. Molecular Biology of the Cell. 6(3): 273-282. 1995.

89. Prusty, D., Park, B.H., Davis, K.E., Farmer, S.R. Activation of MEK/ERK signaling promotes adipogenesis by enhancing peroxisome proliferator-activated receptor gamma (PPARgamma) and C/EBPalpha gene expression during the differentiation of 3T3-L1 preadipocytes. The Journal of Biological Chemistry. 277(48): 46226-46232. 2002.

90. Gong, Z., Niklason, L.E. Small-diameter human vessel wall engineered from bone marrow-derived mesenchymal stem cells (hMSCs). FASEB J. 22(6): 1635-1648. 2008.

91. Hedin, U., Bottger, B.A., Forsberg, E., Johansson, S., Thyberg, J. Diverse effects of fibronectin and laminin on phenotypic properties of cultured arterial smooth muscle cells. The Journal of Cell Biology. 107(1): 307-319. 1988.

92. Tibbitt, M.W., Anseth, K.S. Hydrogels as extracellular matrix mimics for 3D cell culture. Biotechnology and Bioengineering. 103(4): 655-663. 2009.

93. Speer, M.Y., Yang, H.Y., Brabb, T., Leaf, E., Look, A., Lin, W.L., Frutkin, A., Dichek, D., Giachelli, C.M. Smooth muscle cells give rise to osteochondrogenic precursors and chondrocytes in calcifying arteries. Circulation Research. 104(6): 733-741. 2009.

94. Halayko, A.J., Solway, J. Molecular mechanisms of phenotypic plasticity in smooth muscle cells. Journal of Applied Physiology. 90(1): 358-368. 2001.

95. Shanahan, C.M., Cary, N.R., Salisbury, J.R., Proudfoot, D., Weissberg, P.L., Edmonds, M.E. Medial localization of mineralization-regulating proteins in association with Monckeberg's sclerosis: evidence for smooth muscle cell-mediated vascular calcification. Circulation. 100(21): 2168-2176. 1999.

96. Moe, S.M., O'Neill, K.D., Duan, D., Ahmed, S., Chen, N.X., Leapman, S.B., Fineberg, N., Kopecky, K. Medial artery calcification in ESRD patients is associated with deposition of bone matrix proteins. Kidney International. 61(2): 638-647. 2002.

97. Ross, R. Atherosclerosis--an inflammatory disease. The New England Journal of Medicine. 340(2): 115-126. 1999.

98. Lloyd-Jones, D., Adams, R.J., Brown, T.M., Carnethon, M., Dai, S., De Simone, G., Ferguson, T.B., Ford, E., Furie, K., Gillespie, C., Go, A., Greenlund, K., Haase, N., Hailpern, S., Ho, P.M., Howard, V., Kissela, B., Kittner, S., Lackland, D., Lisabeth, L., Marelli, A., McDermott, M.M., Meigs, J., Mozaffarian, D., Mussolino, M., Nichol, G., Roger, V., Rosamond, W., Sacco, R., Sorlie, P., Stafford, R., Thom, T., Wasserthiel-Smoller, S., Wong, N.D., Wylie-Rosett, J.; American Heart Association Statistics Committee and Stroke Statistics Subcommittee. Heart disease and stroke statistics--2010 update: a report from the American Heart Association. Circulation. 121(7):e46-e215. 2010.

99. Nakashima, Y., Fujii, H., Sumiyoshi, S., Wight, T.N., Sueishi, K. Early human atherosclerosis: accumulation of lipid and proteoglycans in intimal thickenings followed by macrophage infiltration. Arterioscler. Thromb. Vasc. Biol. 27(5): 1159-1165. 2007.

100. Khalil, M.F., Wagner, W.D., Goldberg, I.J. Molecular interactions leading to lipoprotein retention and the initiation of atherosclerosis. Arterioscler. Thromb. Vasc. Biol. 24(12): 2211-2218. 2004.

101. Williams, K.J., Tabas, I. The response-to-retention hypothesis of early atherogenesis. Arterioscler. Thromb. Vasc. Biol. 15(5): 551-561. 1995.

102. Camejo, G., Hurt-Camejo, E., Wiklund, O., Bondjers, G. Association of apo B lipoproteins with arterial proteoglycans: pathological significance and molecular basis. Atherosclerosis. 139(2): 205-222. 1998.

103. Vijayagopal, P., Menon, P.V. Varied low density lipoprotein binding property of proteoglycans synthesized by vascular smooth muscle cells cultured on extracellular matrix. Atherosclerosis. 178(1): 75-82. 2005.

104. Katsuda, S., Boyd, H.C., Fligner, C., Ross, R., Gown, A.M. Human atherosclerosis. III. Immunocytochemical analysis of the cell composition of lesions of young adults. Am. J. Pathol. 140(4): 907-914. 1992.

105. Davies, J.D., Carpenter, K.L.H., Challis, I.R., Figg, N.L., McNair, R., Proudfoot, D., Weissberg, P.L., Shanahan, C.M. Adipocytic differentiation and liver X receptor pathways regulate the accumulation of triacylglycerols in human vascular smooth muscle cells. J. Biol. Chem. 280(5): 3911-3919. 2005.

106. Rong, J.X., Shapiro, M., Trogan, E., Fisher, E.A. Transdifferentiation of mouse aortic smooth muscle cells to a macrophage-like state after cholesterol loading. Proc. Natl. Acad. Sci. U. S. A. 100(23): 13531-13536. 2003.

107. Wada, Y., Sugiyama, A., Yamamoto, T., Naito, M., Noguchi, N., Yokoyama, S., Tsujita, M., Kawabe, Y., Kobayashi, M., Izumi, A., Kohro, T., Tanaka, T., Taniguchi, H., Koyama, H., Hirano, K., Yamashita, S., Matsuzawa, Y., Niki, E., Hamakubo, T., Kodama, T. Lipid accumulation in smooth muscle cells under LDL loading is independent of LDL receptor pathway and enhanced by hypoxic conditions. Arterioscler. Thromb. Vasc. Biol. 22(10): 1712-1719. 2002.

108. Papakonstantinou, E., Karakiulakis, G., Eickelberg, O., Perruchoud, A., Block, L., Roth, M. A 340 kDa hyaluronic acid secreted by human vascular smooth muscle cells regulates their proliferation and migration. Glycobiology. 8(8): 821-830. 1998.

109. Stevens, R.L., Colombo, M., Gonzales, J.J., Hollander, W., Schmid, K. The glycosaminoglycans of the human artery and their changes in atherosclerosis. J. Clin. Invest. 58(2): 470-481. 1976.

110. Wagner, W.D. Proteoglycan Structure and Function as Related to Atherosclerosis. Annals of the New York Academy of Sciences. 454: 52-68. 1985.

111. Tammi, M., Seppälä, P.O., Lehtonen, A., Möttönen, M. Connective tissue components in normal and atherosclerotic human coronary arteries. Atherosclerosis 29(2): 191-194. 1978.

112. Theocharis, A.D., Theocharis, D.A., De Luca, G., Hjerpe, A., Karamanos, N.K. Compositional and structural alterations of chondroitin and dermatan sulfates during the progression of atherosclerosis and aneurysmal dilatation of the human abdominal aorta. Biochimie. 84(7): 667-674. 2002.

113. Papakonstantinou, E., Roth, M., Block, L.H., Mirtsou-Fidani, V., Argiriadis, P., Karakiulakis, G. The differential distribution of hyaluronic acid in the layers of human atheromatic aortas is associated with vascular smooth muscle cell proliferation and migration. Atherosclerosis. 138(1): 79-89. 1998.

114. Gombotz, W.R., Wang, G.H., Horbett, T.A., Hoffman, A.S. Protein adsorption to poly(ethylene oxide) surfaces. J. Biomed. Mater. Res. 25(12): 1547-1562. 1991.

115. Munoz-Pinto, D.J., Jimenez-Vergara, A.C., Gelves, L.M., McMahon, R.E., Guiza-Arguello, V., Hahn, M.S. Probing vocal fold fibroblast response to hyaluronan in 3D contexts. Biotechnology and Bioengineering. 104(4): 821-831. 2009.

116. Munoz-Pinto, D.J., Bulick, A.S., Hahn, M.S. Uncoupled investigation of scaffold modulus and mesh size on smooth muscle cell behavior. J. Biomed. Mater. Res. Part A. 90(1): 303-316. 2009.

117. Glukhova, M., Frid, M., Koteliansky, V. Phenotypic changes of human aortic smooth muscle cells during development and in the adult vessel. Am. J. Physiol. 261(4): 78-80. 1991.

118. Raines, E.W., Ross, R. Smooth muscle cells and the pathogenesis of the lesions of atherosclerosis. British Heart Journal. 69(1): S30-37. 1993.

119. Orlandi, A., Bochaton-Piallat, M.-L., Gabbiani, G., Spagnoli, L.G. Aging, smooth muscle cells and vascular pathobiology: implications for atherosclerosis. Atherosclerosis. 188(2): 221-230. 2006.

120. Bobryshev, Y.V., Lord, R.S.A. Langhans cells of human arterial intima: uniform by stellate appearance but different by nature. Tissue and Cell. 28(2): 177-194. 1996.

121. Kruse, R., Merten, M., Buddecke, E., Schmidt, A., Völker, W., Yoshida, K. Cholesterol-dependent changes of glycosaminoglycan pattern in human aorta. Basic Research in Cardiology. 91(5): 344-352. 1996.

122. Hasegawa, H., Kanai, H., Koiwa, Y., Ichiki, M., Tezuka, F. Measurement of elastic moduli of tissue components in atherosclerotic plaques by ultrasonic phased tracking method. Ultrasonics Symposium, 2002. Proceedings. 2002 IEEE, 2: 1847-1850. 2002,

123. Bulick, A.S., Muñoz-Pinto, D.J., Qu, X., Mani, M., Cristancho, D., Urban, M., Hahn, M.S. Impact of endothelial cells and mechanical conditioning on smooth muscle cell extracellular matrix production and differentiation. Tissue Engineering Part A. 15(4): 815-825. 2009.

124. Masters, K.S., Shah, D.N., Leinwand, L.A., Anseth, K.S. Crosslinked hyaluronan scaffolds as a biologically active carrier for valvular interstitial cells. Biomaterials. 26(15): 2517-2525. 2005.

125. Bryant, S.J., Davis-Arehart, K.A., Luo, N., Shoemaker, R.K., Arthur, J.A., Anseth, K.S. Synthesis and characterization of photopolymerized multifunctional hydrogels: Water-soluble poly(vinyl alcohol) and chondroitin sulfate macromers for chondrocyte encapsulation. Macromolecules. 37(18): 6726-6733. 2004.

126. Masters, K.S., Shah, D.N., Walker, G., Leinwand, L.A., Anseth, K.S. Designing scaffolds for valvular interstitial cells: cell adhesion and function on naturally derived materials. J. Biomed. Mater. Res. Part A. 71(1): 172-180. 2004.

127. Benoit, D.S., Anseth, K.S. Heparin functionalized PEG gels that modulate protein adsorption for hMSC adhesion and differentiation. Acta Biomaterialia. 1(4): 461-470. 2005.

128. Benoit, D.S., Durney, A.R., Anseth, K.S. The effect of heparin-functionalized PEG hydrogels on three-dimensional human mesenchymal stem cell osteogenic differentiation. Biomaterials. 28(1): 66-77. 2007.

129. Ford, M.C., Bertram, J.P., Hynes, S.R., Michaud, M., Li, Q., Young, M., Segal, S.S., Madri, J.A., Lavik, E.B. A macroporous hydrogel for the coculture of neural progenitor and endothelial cells to form functional vascular networks in vivo. Proc. Natl. Acad. Sci. U. S. A. 103(8): 2512-2517. 2006.

130. Watkins, A.W., Anseth, K.S. Investigation of molecular transport and distributions in poly(ethylene glycol) hydrogels with confocal laser scanning microscopy. Macromolecules. 38(4): 1326-1334. 2005.

131. Armstrong, J.K., Wenby, R.B., Meiselman, H.J., Fisher, T.C. The hydrodynamic radii of macromolecules and their effect on red blood cell aggregation. Biophysical Journal. 87(6): 4259-4270. 2004.

132. Weirich, J., Seiler, L., Hug, M.J., Fleckenstein-Grün, G. Ca(2+) entry into primary cultured pig coronary smooth muscle cells after previous store depletion by repetitive P2Y purinoceptor stimulation. Cell Calcium. 29(5): 359-367. 2001.

133. Gockerman, A., Clemmons, D.R. Porcine aortic smooth muscle cells secrete a serine protease for insulin-like growth factor binding protein-2. Circ. Res. 76(4): 514-521. 1995.

134. Hahn, M., McHale, M., Wang, E., Schmedlen, R., West, J. Physiologic pulsatile flow bioreactor conditioning of poly(ethylene glycol)-based tissue engineered vascular grafts. Annals of Biomedical Engineering. 35(2): 190-200. 2007.

135. Buxton, A.N., Zhu, J., Marchant, R., West, J.L., Yoo, J.U., Johnstone, B. Design and characterization of poly(Ethylene Glycol) photopolymerizable semi-interpenetrating networks for chondrogenesis of human mesenchymal stem cells. Tissue Engineering. 13(10): 2549-2560. 2007.

136. Gregory, T.R. Nucleotypic effects without nuclei: genome size and erythrocyte size in mammals. Genome. 43(5): 895-901. 2000.

137. Miller, E.J., Gay, S. Collagen: an overview. Methods Enzymol. 82: 3-32. 1982.

138. Luo, Y., Kobler, J.B., Zeitels, S.M., Langer, R. Effects of growth factors on extracellular matrix production by vocal fold fibroblasts in 3-dimensional culture. Tissue Engineering. 12(12): 3365-3374. 2006.

139. Grande-Allen, K.J., Calabro, A., Gupta, V., Wight, T.N., Hascall, V.C., Vesely, I. Glycosaminoglycans and proteoglycans in normal mitral valve leaflets and chordae: association with regions of tensile and compressive loading. Glycobiology. 14(7): 621-633. 2004.

140. Calabro, A., Hascall, V.C., Midura, R.J. Adaptation of FACE methodology for microanalysis of total hyaluronan and chondroitin sulfate composition from cartilage. Glycobiology. 10(3): 283-293. 2000.

141. Hahn, M., Jao, C., Faquin, W., Grande-Allen, K. Glycosaminoglycan composition of the vocal fold lamina propria in relation to function. Annals of Otology, Rhinology, and Laryngology. 117(5): 371-381. 2008.

142. Zhang, G., Wang, X., Wang, Z., Zhang, J., Suggs, L. A PEGylated fibrin patch for mesenchymal stem cell delivery. Tissue Engineering. 12(1): 9-19. 2006.

143. Salinas, C.N., Anseth, K.S. The influence of the RGD peptide motif and its contextual presentation in PEG gels on human mesenchymal stem cell viability. Journal of Tissue Engineering and Regenerative Medicine. 2(5): 296-304. 2008.

144. Burdick, J.A., Anseth, K.S. Photoencapsulation of osteoblasts in injectable RGD-modified PEG hydrogels for bone tissue engineering. Biomaterials. 23(22): 4315-4323. 2002.

145. Salinas, C.N., Anseth, K.S. The enhancement of chondrogenic differentiation of human mesenchymal stem cells by enzymatically regulated RGD functionalities. Biomaterials. 29(15): 2370-2377. 2008.

146. Benoit, D.S.W., Schwartz, M.P., Durney, A.R., Anseth, K.S. Small functional groups for controlled differentiation of hydrogel-encapsulated human mesenchymal stem cells. Nat. Mater. 7(10): 816-823. 2008.

147. Bryant, S.J., Anseth, K.S. Hydrogel properties influence ECM production by chondrocytes photoencapsulated in poly(ethylene glycol) hydrogels. J. Biomed. Mater. Res. 59(1): 63-72. 2002.

148. Bryant, S.J., Anseth, K.S. Controlling the spatial distribution of ECM components in degradable PEG hydrogels for tissue engineering cartilage. J. Biomed. Mater. Res. Part A. 64(1): 70-79. 2003.

149. Munoz-Pinto, D.J., McMahon, R.E., Kanzelberger, M.A., Jimenez-Vergara, A.C., Grunlan, M.A., Hahn, M.S. Inorganic-organic hybrid scaffolds for osteochondral regeneration. J. Biomed. Mater. Res. Part A. 94(1): 112-121. 2010.

150. Liao, H., Munoz-Pinto, D., Qu, X., Hou, Y., Grunlan, M., Hahn, M. Influence of hydrogel material properties on vocal fold fibroblast extracellular matrix production and phenotype. Acta Biomateralia. 4(5): 1161-1171. 2008.

151. Bryant, S.J., Durand, K.L., Anseth, K.S. Manipulations in hydrogel chemistry control photoencapsulated chondrocyte behavior and their extracellular matrix production. J. Biomed. Mater. Res. Part A. 67A(4): 1430-1436. 2003.

152. Peyton, S., Raub, C., Keschrumrus, V., Putnam, A. The use of poly(ethylene glycol) hydrogels to investigate the impact of ECM chemistry and mechanics on smooth muscle cells. Biomaterials 27(28): 4881-4893. 2006.

153. Zhang, Z., Apse, K., Pang, J., Stanton, R.C. High glucose inhibits glucose-6-phosphate dehydrogenase via cAMP in aortic endothelial cells. J. Biol. Chem. 275: 40042-40047. 2000.

154. Goodrich, R.P., Sowemimo-Coker, S.O., Zerez, C.R., Tanaka, K.R. Preservation of metabolic activity in lyophilized human erythrocytes. Proc. Natl. Acad. Sci. U. S. A. 89(3): 967-971. 1992.

155. Keeley, F., Todorovich, L., Rabinovitch, M. Elastin and elastases in the pathology of the arterial wall. In: Robert, L., and Hornebeck, W., eds. Elastin and elastases. pp. 169-184. Boca Raton: CRC Press. 1989.

156. Andreeva, E.R., Pugach, I.M., Orekhov, A.N. Collagen-synthesizing cells in initial and advanced atherosclerotic lesions of human aorta. Atherosclerosis. 130(1-2): 133-142. 1997.

157. Kratky, R.G., Ivey, J., Roach, M.R. Local changes in collagen content in rabbit aortic atherosclerotic lesions with time. Atherosclerosis. 143(1): 7-14. 1999.

158. Handa, S., Sadi, A.M., Cybulsky, M.I., Stewart, D.J., Husain, M. Region-specific patterns of vascular remodelling occur early in atherosclerosis and without loss of smooth muscle cell markers. Atherosclerosis. 196(2): 617-623. 2008.

159. Adiguzel, E., Ahmad, P.J., Franco, C., Bendeck, M.P. Collagens in the progression and complications of atherosclerosis. Vascular Medicine. 14(1): 73-89. 2009.

160. Gutierrez, P., O'Brien, K.D., Ferguson, M., Nikkari, T., Alpers, C.E., Wight, T.N. Differences in the distribution of versican, decorin, and biglycan in atherosclerotic human coronary arteries. Cardiovascular Pathology. 6(5): 271-278. 1997.

161. Wight, T.N., Merrilees, M.J. Proteoglycans in atherosclerosis and restenosis: key roles for versican. Circ. Res. 94(9): 1158-1167. 2004.

162. O'Brien, K.D., Olin, K.L., Alpers, C.E., Chiu, W., Ferguson, M., Hudkins, K., Wight, T.N., Chait, A. Comparison of apolipoprotein and proteoglycan deposits in human coronary atherosclerotic plaques : colocalization of biglycan with apolipoproteins. Circulation. 98(6): 519-527. 1998.

163. Evanko, S., Raines, E., Ross, R., Gold, L., Wight, T. Proteoglycan distribution in lesions of atherosclerosis depends on lesion severity, structural characteristics, and the proximity of platelet-derived growth factor and transforming growth factor-beta. Am. J. Pathol. 152(2): 533-546. 1998.

164. Rodriguez-Lee, M., Ostergren-Lunden, G., Wallin, B., Moses, J., Bondjers, G., Camejo, G. Fatty acids cause alterations of human arterial smooth muscle cell proteoglycans that increase the affinity for low-density lipoprotein. Arterioscler. Thromb. Vasc. Biol. 26(1): 130-135. 2006.

165. McBeath, R., Pirone, D.M., Nelson, C.M., Bhadriraju, K., Chen, C.S. Cell shape, cytoskeletal tension, and RhoA regulate stem cell lineage commitment. Developmental Cell 6(4): 483-495. 2004.

166. Hahn, M.S., Miller, J.S., West, J.L. Laser scanning lithography for surface micropatterning on hydrogels. Advanced Materials. 17(24). 2939-2942. 2005.

167. Hahn, M.S., Taite, L.J., Moon, J.J., Rowland, M.C., Ruffino, K.A., West, J.L. Photolithographic patterning of polyethylene glycol hydrogels. Biomaterials. 27(12): 2519-2524. 2006.

VITA

Name: Xin Qu

Address: 200 Jack E Brown Building
3122 TAMU
College Station, TX 77843-3122

Email Address: quxinwly@hotmail.com

Education: B.S., Life Sciences, University of Science and Technology of China, 2006

Publications:

X. Qu, A.C Jimenez-Vergara, D.J. Munoz-Pinto, D. Ortiz, R.E. McMahon, D Cristancho, S. Becerra-Bayona, V. Guiza-Arguello, K.J. Grande-Allen, M.S. Hahn. Regulation of smooth muscle cell phenotype by glycosaminoglycan identity. Acta Biomaterialia. 7(3): 1031-1039. 2011.

R.E. McMahon*****, **X. Qu***, A.C. Jimenez-Vergara, C.A. Bashur, S.A. Guelcher, A.S. Goldstein, M.S. Hahn. Electrospun mesh hydrogel composites for tissue engineered vascular grafts. Tissue Engineering Part C. 17(4): 451-461. 2011.

H. Liao, D. Munoz-Pinto, **X. Qu,** Y. Hou, M. Grunlan, M.S. Hahn. Influence of hydrogel mechanical properties and mesh size on vocal fold fibroblast extracellular matrix production. Acta Biomaterialia. 4(5): 1161-1171. 2008.

A. Bulick, D. Munoz-Pinto, **X. Qu,** M. Mani, D.Cristancho, M.Urban, M.S. Hahn. Impact of endothelial cells and mechanical conditioning on smooth muscle cell extracellular matrix production and differentiation. Tissue Engineering. 15(4):815-825. 2009.

*Authors contributed equally to this work